

SHIELD: Secure Hypernetworks for Incremental Expansion Learning Defense

Patryk Krukowski^{1,2} Łukasz Gorczyca¹ Piotr Helm¹
Kamil Książek¹ Przemysław Spurek^{1,3}
patryk.krukowski@doctoral.uj.edu.pl

¹Jagiellonian University ²IDEAS NCBR ³ IDEAS Research Institute

Abstract

Continual learning under adversarial conditions remains an open problem, as existing methods often compromise either robustness, scalability, or both. We propose a novel framework that integrates Interval Bound Propagation (IBP) with a hypernetwork-based architecture to enable certifiably robust continual learning across sequential tasks. Our method, SHIELD, generates task-specific model parameters via a shared hypernetwork conditioned solely on compact task embeddings, eliminating the need for replay buffers or full model copies and enabling efficient over time. To further enhance robustness, we introduce Interval MixUp, a novel training strategy that blends virtual examples represented as ℓ_∞ balls centered around MixUp points. Leveraging interval arithmetic, this technique guarantees certified robustness while mitigating the wrapping effect, resulting in smoother decision boundaries. We evaluate SHIELD under strong white-box adversarial attacks, including PGD and AutoAttack, across multiple benchmarks. It consistently outperforms existing robust continual learning methods, achieving state-of-the-art average accuracy while maintaining both scalability and certification. These results represent a significant step toward practical and theoretically grounded continual learning in adversarial settings.

1 Introduction

Deep neural networks have achieved remarkable performance across a wide range of tasks, often surpassing human-level accuracy (He et al. 2016). However, their success hinges on static training settings that do not reflect how intelligent systems are expected to operate in the real world. In practice, models must continually adapt to changing conditions while retaining prior knowledge, a challenge known as continual learning (McCloskey and Cohen 1989; Hsu et al. 2018). At the same time, these models remain highly vulnerable to adversarial perturbations; small, carefully crafted input changes that can cause confident but incorrect predictions (Szegedy et al. 2013; Goodfellow, Shlens, and Szegedy 2014). This vulnerability raises serious concerns in high-stakes applications such as autonomous driving, robotics, and healthcare, where both adaptability and robustness are essential for safety and trust.

Surprisingly, most research treats these challenges in isolation. This disconnect is striking, given that real-world AI systems must not only learn and adapt continuously but also resist adversarial manipulation over time. Consider an autonomous vehicle that incrementally learns to navigate unfamiliar roads or environments. As it learns on the go, it must remain robust against adversarial threats like deceptive road signs, tampered traffic signals, and sensor manipulations that aim to mislead it. Without such resilience, this adaptive learning could become a critical vulnerability instead of an asset.

Despite its importance, this intersection of continual learning and adversarial robustness remains highly underexplored. Existing approaches that attempt to bridge this gap are limited. AIR (Zhou and Hua 2024), for example, uses unsupervised data augmentations to promote robustness during continual learning, but it is only demonstrated on short task sequences and cannot scale to more complex benchmarks. Double Gradient Projection (DGP) (Ru et al. 2024) enhances robustness by constraining weight updates; however, it necessitates storing large amounts of per-task gradient information. This makes it impractical for large-scale datasets or modern architectures. Moreover, this storage requirement introduces privacy concerns, especially in domains where task data is sensitive and cannot be retained.

To address these limitations, we introduce a new framework for adversarially robust continual learning. Our method uses a shared hypernetwork to generate task-specific model parameters from compact, trainable embeddings. This architecture enables efficient adaptation to new tasks without requiring replay buffers, gradient logs, or full model snapshots, thus ensuring scalability and privacy. To defend against adversarial inputs, we integrate Interval Bound Propagation (IBP) (Gowal et al. 2018), which provides formal robustness guarantees by accounting for worst-case input perturbations. We further introduce Interval MixUp, a novel technique that extends traditional MixUp by interpolating not individual input samples, but uncertainty-aware regions in the input space, enhancing robustness during training. The standard MixUp strategy is unsuitable in our

setting, as training on samples with excessively large perturbation radii degrades model performance. To mitigate this, we constrain the hypercube volume near decision boundaries and employ a weighted cross-entropy loss. Empirical results demonstrate that Interval MixUp is essential for achieving high-performing models.

Together, these components form a unified and efficient framework for continual learning in the presence of adversarial threats. By jointly addressing the challenges of continual adaptation and certifiable robustness, our approach takes a significant step toward building safe, trustworthy, and lifelong learning AI systems capable of operating reliably in complex, dynamic environments. An overview of our method is illustrated in Figure 1.

The key contributions of this work are as follows:

- We propose SHIELD¹, a novel architecture for robust continual learning that unifies certified adversarial robustness with strong sequential task performance.
- Our method integrates IBP into a hypernetwork architecture and introduces Interval MixUp, a novel training strategy blending virtual interpolation and interval arithmetic to widen decision boundaries and enhance robustness.
- SHIELD is attack-agnostic and achieves state-of-the-art or highly competitive results on multiple continual learning benchmarks, including Split miniImageNet, with up to 2× higher adversarial accuracy than prior methods.

2 Related Works

Continual learning and adversarial robustness have largely been studied in isolation, with only a few attempts to bridge the two (see Appendix A for an in-depth overview). Recent work has begun to expose the vulnerabilities of continual learning models to adversarial attacks. For example, (Khan et al. 2022) evaluates several continual learning methods under adversarial scenarios, highlighting the need for joint treatment of robustness and forgetting. AIR (Zhou and Hua 2024) offers one such integrated approach using unsupervised data augmentations for adversarial defense, though its effectiveness is limited to short task sequences.

Gradient-based methods like GEM (Lopez-Paz and Ranzato 2017) and GPM (Saha, Garg, and Roy 2021) primarily aim to prevent forgetting by using episodic memory and subspace projections, respectively, but do not explicitly address adversarial robustness. DGP (Ru et al. 2024), built as an extension of GPM, further refines these projections to maintain stability across tasks. Interestingly, the authors of DGP observe that while their method improves continual learning performance, the projection strategy itself makes the model more susceptible to adversarial attacks, revealing a critical

trade-off between preserving past knowledge and ensuring robustness.

Crucially, none of these methods explore hypernetworks (Ha, Dai, and Le 2016), despite their proven benefits in continual learning (Henning et al. 2021; Książek and Spurek 2023; Wang et al. 2024) for achieving modular task representations.

3 SHIELD: Secure Hypernetworks for Incremental Expansion Learning Defense

In this section, we introduce SHIELD, a model designed for continual adversarial defense across a sequence of tasks. SHIELD comprises two primary components: a hypernetwork that generates task-specific parameters and a target network that leverages interval arithmetic to enable certified robustness. We begin by outlining the overall architecture, followed by a formal definition of certified robustness in neural networks. We then demonstrate how SHIELD meets these criteria.

SHIELD Architecture

Hypernetwork Our model uses trainable embeddings $e_t \in \mathbb{R}^N$, where $t \in \{1, \dots, T\}$ represents consecutive tasks indices and T is its total number. These vectors serve as the input to the hypernetwork, which produces the task-dedicated target network weights. More specifically, the hypernetwork \mathcal{H} with weights Φ generates weights θ_t of the target network f , designed for the t -th task, i.e. $\mathcal{H}(e_t; \Phi) = \theta_t$. Therefore, the target network is not trained directly, and the meta-architecture generates distinct weights for each continual learning task. The function $f_{\theta_t} : X \rightarrow Y$ predicts labels Y for data samples X based on weights θ_t . Finally, each continual learning task is represented by a classifier function

$$f_{\theta_t}(\cdot) = f(\cdot; \theta_t) = f(\cdot; \mathcal{H}(e_t; \Phi)). \quad (1)$$

After training, a single meta-model produces distinct task-specific weights, effectively minimizing forgetting.

Target network In SHIELD, the target network is designed for interval representation of input points instead of single real values. In practice, we use the IBP approach (Gowal et al. 2018; Morawiecki et al. 2019) in the target model. Instead of utilizing a single-valued point $x = (x_1, \dots, x_d) \in \mathbb{R}^d$ as input to the target model f_{θ_t} , we propagate a d -dimensional hypercube:

$$I_\varepsilon(x) = [x_1 - \varepsilon, x_1 + \varepsilon] \times \dots \times [x_d - \varepsilon, x_d + \varepsilon], \quad (2)$$

where $\varepsilon \geq 0$. When we consider a target model f_{θ_t} , it is composed of K layers defined by the transformations

$$z_k = h_k(z_{k-1}) = W_k z_{k-1} + b_k, \quad \text{for } k = 2, \dots, K, \quad (3)$$

$$z_1 = x. \quad (4)$$

In practice, the transformations h_k are connected by non-linear, non-decreasing activation functions such as

¹Code available at: <https://github.com/pkrukowski1/SHIELD>

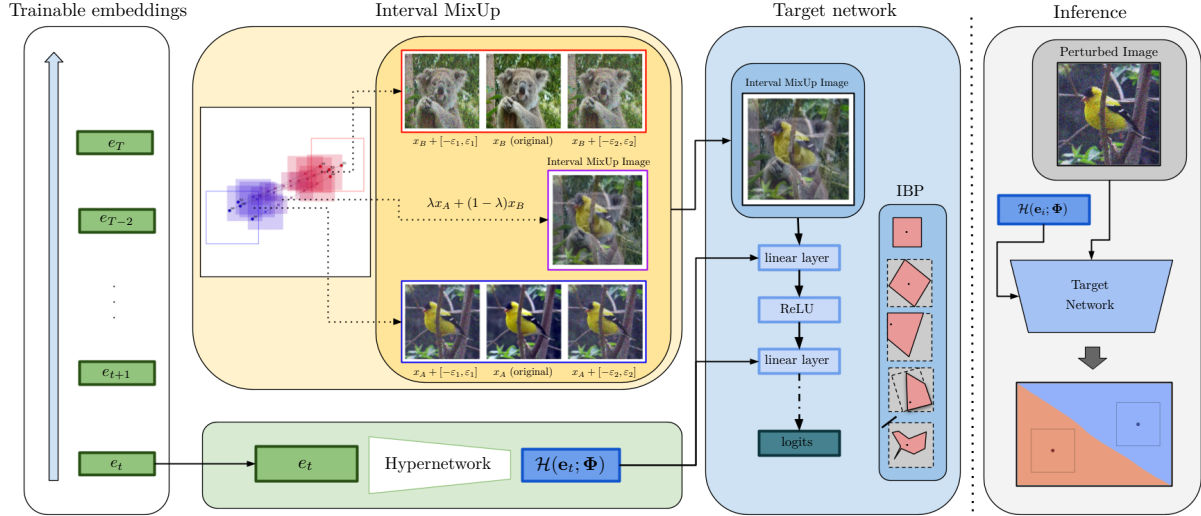


Figure 1: SHIELD uses a hypernetwork to map task-specific embeddings \mathbf{e}_t into target models that propagate virtual Interval MixUp hypercubes, enabling robust multi-task learning and certified adversarial resistance. In the Interval MixUp visualization, edge images are perturbed, the center is unperturbed, and the IBP column shows how the input hypercube is transformed across network layers.

ReLU or sigmoid, so that each layer consists of an affine mapping followed by a non-linearity. For clarity of exposition, we express each h_k in affine form only in Eq. (3). In the IBP approach (Gowal et al. 2018), in each layer, we find the smallest bounding box that encloses the transformed output of the previous layer. To bound the activation z_k of the k -th layer in a neural network, we compute an axis-aligned hypercube $[\underline{z}_k, \bar{z}_k]$, where \underline{z}_k and \bar{z}_k represent the element-wise lower and upper bounds, respectively. This hypercube can be written as:

$$I_\epsilon(z_k) = [\underline{z}_k, \bar{z}_k] = [\underline{z}_{k,1}, \bar{z}_{k,1}] \times \dots \times [\underline{z}_{k,d_k}, \bar{z}_{k,d_k}], \quad (5)$$

where d_k is the output dimension of the k -th layer.

To propagate such intervals efficiently through the layers of a neural network, we use interval arithmetic, leveraging a midpoint-radius representation. This strategy enables efficient and scalable computations. Specifically, by applying Equation (3) to the input hypercube $[\underline{z}_{k-1}, \bar{z}_{k-1}]$, we define:

$$\begin{aligned} \mu_{k-1} &= \frac{\bar{z}_{k-1} + \underline{z}_{k-1}}{2}, & r_{k-1} &= \frac{\bar{z}_{k-1} - \underline{z}_{k-1}}{2}, \\ \mu_k &= W_k \mu_{k-1} + b_k, & r_k &= |W_k| r_{k-1}, \\ \underline{z}_k^* &= \mu_k - r_k, & \bar{z}_k^* &= \mu_k + r_k, \end{aligned} \quad (6)$$

where $|\cdot|$ denotes the element-wise absolute value operator. The resulting hypercube $[\underline{z}_k^*, \bar{z}_k^*]$ serves as the input to the next activation function. For a monotonic non-decreasing activation function $g(\cdot)$, the final output bounds after applying the activation are given by:

$$\underline{z}_k = g(\underline{z}_k^*), \quad \bar{z}_k = g(\bar{z}_k^*). \quad (7)$$

This procedure, known as IBP, enables tractable, layer-wise propagation of bounds through the entire network.

To ensure robust classification, we adopt a worst-case loss function during training (see Equation (8)) that accounts for the entire interval bound $[\underline{z}_K, \bar{z}_K]$ of the final logits. This encourages the model to make consistent predictions for all inputs within a certified neighborhood of the original sample.

The goal is to guarantee that the model correctly classifies not only the input sample x , but also all perturbed samples \hat{x} within the ϵ -bounded ℓ_∞ hypercube, i.e., for all $\hat{x} \in [x - \epsilon, x + \epsilon]$. This ensures that the predicted class remains unchanged within a specified neighborhood around the input, providing certified robustness against adversarial perturbations.

Ultimately, the model comprises a learnable embedding and a hypernetwork designed to create the IBP-based target model for a given task. Therefore, SHIELD has improved robustness against adversarial attacks.

SHIELD Loss Function

One of the core components of our model is the loss function, which simultaneously mitigates catastrophic forgetting and enhances robustness against adversarial attacks. We adopt a worst-case loss computed over the interval bounds $[\underline{z}_K, \bar{z}_K]$ of the final logits. This approach ensures that the entire output bounding box is classified correctly, meaning that all permissible input perturbations within the specified interval do not alter the predicted class.

Concretely, the logits corresponding to the true class y_{true} and the predicted class \hat{y} are considered as its lower bound, while the logits of all other classes are set to

their respective upper bounds:

$$\hat{z}_{K,\hat{y}} = \begin{cases} \bar{z}_K, & \text{for } \hat{y} \neq y_{\text{true}}, \\ \underline{z}_K, & \text{otherwise.} \end{cases} \quad (8)$$

This selection of bounds yields the most pessimistic, interval-based prediction vector, effectively capturing the worst-case scenario within the certified neighborhood. We then apply the softmax function and the cross-entropy loss to $\hat{z}_{K,\hat{y}}$.

As shown in (Gowal et al. 2018), computing these interval bounds requires only two forward passes through the network, making the method computationally practical. To address the challenge of overly loose bounds in complex networks, the authors of (Gowal et al. 2018) proposed a combined loss that blends the standard cross-entropy loss on the nominal inputs with the interval-based worst-case loss:

$$\mathcal{L}_{\text{IBP}} = \kappa \cdot \mathcal{L}_{\text{CE}}(\sigma(\hat{y}), y_{\text{true}}) + (1-\kappa) \cdot \mathcal{L}_{\text{CE}}(\sigma(\hat{z}_{K,\hat{y}}), y_{\text{true}}), \quad (9)$$

where \mathcal{L}_{CE} denotes the cross-entropy loss, $\sigma(\cdot)$ is a softmax function, and $\kappa \in [0, 1]$ balances the trade-off. For the sake of simplicity, we omit arguments of \mathcal{L}_{IBP} . Notably, when $\varepsilon = 0$, the interval bounds collapse to point predictions and \mathcal{L}_{IBP} reduces to the standard cross-entropy loss. To facilitate stable optimization during training, we apply a scheduled annealing of κ , detailed in Appendix G.

Although ensuring adversarial robustness is possible under worst-case accuracy conditions, it is also essential to avoid catastrophic forgetting in the hypernetwork. Consequently, we incorporate a regularization term responsible for maintaining knowledge from previous continual learning tasks, as in (von Oswald et al. 2019). Therefore, we can compare the fixed hypernetwork output (i.e. the target network weights) that was generated before learning the current task $t_c \in \{2, \dots, T\}$, denoted by Φ^* , with the hypernetwork output after recent suggestions for its weight changes, $\Phi + \Delta\Phi$. Ultimately, in SHIELD, the formula for the regularization loss is presented as:

$$\mathcal{L}_{\text{out}} = \frac{1}{t_c - 1} \cdot \sum_{t=1}^{t_c-1} \|\mathcal{H}(\mathbf{e}_t; \Phi^*) - \mathcal{H}(\mathbf{e}_t; \Phi + \Delta\Phi)\|^2. \quad (10)$$

The final loss function consists of the \mathcal{L}_{IBP} loss and hypernetwork regularization term \mathcal{L}_{out} :

$$\mathcal{L}_{\text{total}} = \mathcal{L}_{\text{IBP}} + \beta \cdot \mathcal{L}_{\text{out}} \quad (11)$$

where $\beta > 0$ is a hyperparameter that influences the stability of the hypernetwork.

Robustness Guarantees of SHIELD

In this subsection, we provide theoretical justification for the certified robustness properties achieved via IBP in SHIELD. We first formalize certified robustness for standard feedforward networks, then extend the concept to the continual learning setting, and finally apply it to our proposed method.

Definition 3.1 (Certified Robustness). Let y_{true} be the true class of an input sample $x \in \mathbb{R}^d$. A classifier f_{θ} parametrized by θ is certifiably robust at x under ℓ_{∞} perturbations of radius ε if:

$$\underline{z}_{y_{\text{true}}}^{(K)}(x; \theta_t) > \max_{j \neq y_{\text{true}}} \bar{z}_j^{(K)}(x; \theta_t), \quad (12)$$

for all the samples from the perturbation set $\{x + \delta : \|\delta\|_{\infty} \leq \varepsilon\}$, where $\underline{z}^{(K)}$, $\bar{z}^{(K)}$ are lower and upper bounds, respectively, on the output logits for x at the final layer K , computed using IBP.

Definition 3.2 (Certified Robustness in Continual Learning). Consider a continual learning setup with a sequence of T tasks, $\{\mathcal{D}_t\}_{t=1}^T$, where each task dataset $\mathcal{D}_t = \{(x_i^{(t)}, y_i^{(t)})\}_{i=1}^{N_t}$ is drawn from a task-specific distribution $P_t(x, y)$. Let θ_t denote the model parameters after learning task t . The model is said to be certifiably robust up to time t if, for all samples $(x, y_{\text{true}}) \in \bigcup_{s=1}^t \mathcal{D}_s$, the following condition holds:

$$\underline{z}_{y_{\text{true}}}^{(K)}(x; \theta_t) > \max_{j \neq y_{\text{true}}} \bar{z}_j^{(K)}(x; \theta_t), \quad \text{for all } \|\delta\|_{\infty} \leq \varepsilon. \quad (13)$$

This condition guarantees that the model’s predictions remain robust to bounded adversarial perturbations across all tasks encountered so far, without requiring access to the full datasets $\{\mathcal{D}_t\}_{t=1}^T$.

SHIELD is designed to meet this robustness criterion by integrating IBP-based training within a hypernetwork-based continual learning framework. Specifically, we verify that for any task $s \leq t$ and any sample $(x, y_{\text{true}}) \in \mathcal{D}_s$, Equation (13) holds at any time t , ensuring robustness to perturbations within an ε -bounded ℓ_{∞} -norm.

In our approach, the hypernetwork generates task-specific parameters $\theta_t = \mathcal{H}(\mathbf{e}_t; \Phi)$ for the target network f_{θ_t} . We train the hypernetwork using IBP to minimize the certified loss, as outlined in Equation (9). This training procedure encourages each task-specific model to be certifiably robust within its assigned interval bounds. To mitigate forgetting and support robustness across tasks, the regularization term in Equation (10) promotes consistency with previously generated task parameters. As a result, our method supports the accumulation of certified robustness across tasks throughout continual learning.

Assuming effective optimization of both the certified loss and the regularization term, the resulting model f_{θ_t} satisfies $\underline{z}_{y_{\text{true}}}^{(K)}(x; \theta_t) > \max_{j \neq y_{\text{true}}} \bar{z}_j^{(K)}(x; \theta_t)$, for all samples (x, y_{true}) from the combined datasets $\bigcup_{s=1}^t \mathcal{D}_s$ and all perturbations $\|\delta\|_{\infty} \leq \varepsilon$.

4 Enhancing Certified Robustness of SHIELD via Interval MixUp

In this section, we revisit the MixUp technique (Zhang et al. 2018a) and adapt it to align with interval arithmetic and continual learning. We then demonstrate that

our interval-based MixUp approach enhances the robustness of our method by encouraging the decision boundary to move as far as possible from intervals to be correctly classified, without sacrificing accuracy.

MixUp MixUp (Zhang et al. 2018a) improves model generalization by training on convex combinations of input samples and their corresponding labels. Instead of optimizing the model on individual examples, MixUp introduces synthetic points that lie along linear paths between pairs of training samples. This encourages the model to behave smoothly between classes and to avoid overly confident or abrupt predictions in regions where data support is lacking.

MixUp introduces an inductive bias that promotes linear behavior between training examples. It smooths the model’s decision surface, reduces memorization of noisy labels, and improves generalization. By enforcing consistency across interpolated inputs and outputs, it also enhances robustness to ambiguous or uncertain regions in the input space. We present more technical details on MixUp in Appendix B.

Interval MixUp To enable the benefits of MixUp in the context of certified training, we introduce an extension called Interval MixUp, which operates directly on interval-bounded inputs as defined in Interval Bound Propagation (IBP). Unlike standard MixUp that interpolates between individual input points, Interval MixUp interpolates entire ℓ_∞ -bounded perturbation sets, represented as hypercubes, resulting in virtual inputs with smooth certified regions and continuous transitions across class boundaries.

Importantly, our method deviates from the standard MixUp formulation by avoiding label interpolation. Instead, it performs interpolation at the loss level by computing the cross-entropy loss on virtual inputs and weighting the individual loss terms using the MixUp coefficient. This leads to a principled formulation that remains compatible with the requirements of certified training.

First, we construct a virtual sample by linearly interpolating between the midpoints of two original ℓ_∞ -bounded hypercubes. This yields a new hypercube centered at the interpolated point, which remains a valid input region and can be propagated through the network using standard IBP-based methods. To complete the definition of this virtual region, we must also specify its radius.

Optimizing the IBP loss under large perturbation radii ε is difficult due to unstable gradients, overly loose interval bounds, and excessive over-approximation of the certified region. These challenges often result in degraded training dynamics and suboptimal convergence. However, applying large perturbations to virtual points that lie far from the original data manifold is unnecessary and can even be harmful. To address this, we propose a simple yet effective strategy: define the radius of the new hypercube as a function of its distance from the original data. Specifically, we reduce the per-

turbation radius as the interpolated point moves farther away from its endpoints. Let $\lambda \in [0, 1]$ denote the MixUp mixing coefficient. The adjusted perturbation radius is then defined as:

$$\varepsilon' = |2\lambda - 1| \cdot \varepsilon, \quad (14)$$

which smoothly scales the certified region depending on the location of the virtual sample between its source points.

This formulation yields the maximum radius when λ is close to 0 or 1, i.e., when the virtual sample is close to one of the original points, and reduces it to zero when $\lambda = 0.5$, i.e., when the sample is equidistant and lies furthest from either original data point. This leads to a smoothed decision boundary and more stable training while maintaining robustness near the data manifold. In Appendix H, we explore the influence of different transformations in Equation (14) (such as linear, quadratic, logarithmic, and cosine ones) on the training process and defense against adversarial attacks.

Furthermore, both the forward and backward passes in Interval MixUp are performed solely on virtual, interval-bounded examples obtained by interpolating pairs of inputs. As a result, the propagated hypercubes (i.e., interval bounds around the inputs) have smaller radii than those centered at the original data points. This has a crucial side effect: it mitigates the wrapping effect (Neumaier 1993), a well-known limitation of interval arithmetic. The wrapping effect arises when high-dimensional intervals are passed through non-linear layers of the neural network, causing them to grow excessively and become increasingly misaligned with the true shape of the reachable set. This over-approximation results in looser, overly conservative bounds that may significantly underestimate the model’s actual robustness.

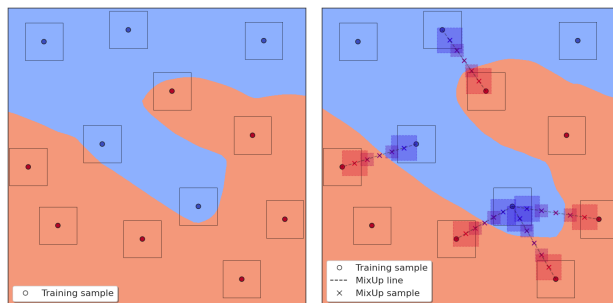


Figure 2: (left side) Without Interval MixUp: Training leads to sharper boundaries and poor robustness across class transitions. (right side) With Interval MixUp: Interpolated samples (\times) with scaled certified regions (boxes) encourage smooth transitions and robust boundaries.

To build intuition for how Interval MixUp operates in practice, we construct a 2D toy experiment, visualized in Figure 2. We generate synthetic training data consisting of a few points from two distinct classes, randomly placed within the unit square $[0, 1]^2$. Each point

is associated with a certified region, shown as a square representing an ℓ_∞ -bounded hypercube.

We then identify several pairs of nearby points belonging to opposite classes. For each such pair, we apply Interval MixUp by linearly interpolating the bounds of their certified regions using a mixing coefficient $\lambda \in [0, 1]$. This produces a set of virtual samples along the line connecting each pair. These samples are visualized as \times markers colored by their interpolation ratio, ranging from red (class 0) to blue (class 1), with intermediate hues indicating mixed contributions. Each virtual point is surrounded by a semi-transparent certified box, whose size is adjusted using Equation (14). We train SHIELD model on this setup using only the Interval MixUp samples. The resulting decision surface and certified regions, shown in Figure 2, illustrate how Interval MixUp helps populate the space between classes, guiding the decision boundary away from both the real data.

By interpolating smaller virtual hypercubes, Interval MixUp reduces the growth of these intervals during propagation, thereby maintaining tighter and more informative bounds. This is illustrated in Figure 3, which reports verified accuracy (Zhang et al. 2018b). Verified accuracy measures whether a model is not only correct on a given input but also robust to all perturbations within a specified ε -ball around it, unlike classical accuracy, which only evaluates predictions on clean, unperturbed data. Verified accuracy thus reflects a model’s certified robustness by leveraging the interval bounds computed during training.

Importantly, models trained with Interval MixUp achieve significantly higher verified accuracy compared to those trained with standard IBP, and their verified accuracy closely matches their classical accuracy (see Figure 3). As a consequence, these models outperform standard IBP baselines and are more resilient to adversarial attacks evaluated in this paper. All reported results are based on the best-performing models selected using a single random seed. Moreover, we present examples of Interval MixUp samples in Appendix M.

SHIELD Loss Function with Interval MixUp

When applying Interval MixUp in SHIELD, we cannot directly use Equation (9), as the original input data is replaced by virtual samples generated through the interpolation of input pairs. To accommodate this, we introduce a reformulated loss function designed specifically for these synthetic samples.

Following the standard MixUp framework, we first adapt the cross-entropy loss to account for mixed labels. The MixUp loss is defined as:

$$\begin{aligned} \mathcal{L}_{\text{MixUp}}(\tilde{x}, y_a, y_b) &= \lambda \mathcal{L}_{\text{CE}}(\sigma(f(\tilde{x}); \theta_t), y_a) \\ &+ (1 - \lambda) \mathcal{L}_{\text{CE}}(\sigma(f(\tilde{x}); \theta_t), y_b) \end{aligned} \quad (15)$$

where $f(\cdot; \theta_t)$ denotes the neural network, $\tilde{x} = \lambda x_a + (1 - \lambda)x_b$ is the interpolated input sample, and y_a, y_b are the corresponding one-hot labels for x_a and x_b , respectively. To integrate certified robustness into this formulation, we extend the loss to an interval-based version.

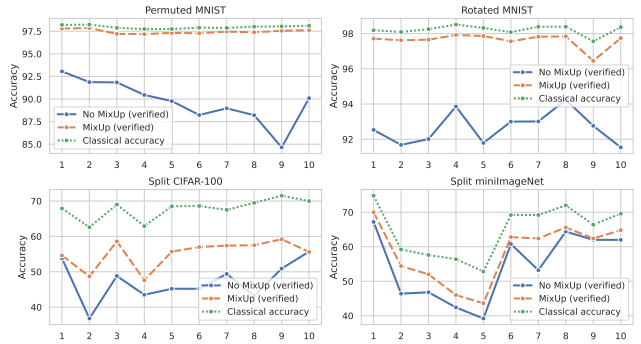


Figure 3: Comparison of verified accuracy and classical accuracy across four continual learning benchmarks: Permuted MNIST, Rotated MNIST, Split CIFAR-100, and Split miniImageNet. For each task, we report the AA metric after sequentially learning all preceding tasks.

The resulting Interval MixUp loss is:

$$\begin{aligned} \mathcal{L}_{\text{IMixUp}} &= \kappa \cdot \mathcal{L}_{\text{MixUp}}(\tilde{x}, y_a, y_b) \\ &+ (1 - \kappa) \cdot \hat{\mathcal{L}}_{\text{MixUp}}([\tilde{x} - \varepsilon', \tilde{x} + \varepsilon'], y_a, y_b), \end{aligned} \quad (16)$$

where ε' is the scaled perturbation radius (see Equation (14)), and $\kappa \in [0, 1]$ balances the standard and certified components of the loss. We omit arguments of $\mathcal{L}_{\text{IMixUp}}$ to simplify the notation. The term $\hat{\mathcal{L}}_{\text{MixUp}}$ is defined as:

$$\begin{aligned} \hat{\mathcal{L}}_{\text{MixUp}}([\tilde{x} - \varepsilon', \tilde{x} + \varepsilon'], y_a, y_b) &= \lambda \cdot \mathcal{L}_{\text{CE}}(\sigma(\hat{z}_{K, \hat{y}_a}), y_a) \\ &+ (1 - \lambda) \cdot \mathcal{L}_{\text{CE}}(\sigma(\hat{z}_{K, \hat{y}_b}), y_b), \end{aligned} \quad (17)$$

where \hat{z}_{K, \hat{y}_a} and \hat{z}_{K, \hat{y}_b} denote the components of the target network’s interval output associated with classes \hat{y}_a and \hat{y}_b , respectively, after K transformations, as specified in Equation (8). This formulation enables us to retain certified robustness guarantees even for interpolated virtual samples, allowing us to benefit from MixUp’s generalization while maintaining interval-based certification.

Finally, to adapt Interval MixUp to the continual learning setting, we incorporate it into the overall objective by combining it with the hypernetwork regularization term from Equation (10). The complete loss function becomes:

$$\mathcal{L}_{\text{total}} = \mathcal{L}_{\text{IMixUp}} + \beta \cdot \mathcal{L}_{\text{out}}, \quad (18)$$

where β is a hyperparameter controlling the strength of the hypernetwork regularization, and \mathcal{L}_{out} is defined as in Equation (10). This final formulation ensures that our model can learn robust, certified representations in the context of continual learning. The training algorithm of our method is provided in Appendix K.

5 Experiments

This section outlines the experimental setup and results for SHIELD. We describe the datasets used, along with

the architectures of both the target network and the hypernetwork. All experiments are conducted in a Task-Incremental Learning setting, where the task identity is known to the model during both training and evaluation. Moreover, our method naturally extends to the Class-Incremental Learning (CIL) scenario, retaining a significant level of adversarial robustness. Appendix J shows that SHIELD consistently outperforms a strong baseline under various attacks in the CIL scenario.

Benchmarks To assess the effectiveness of our approach, we perform experiments on four standard benchmarks: Permuted MNIST, Rotated MNIST, Split CIFAR-100, and Split miniImageNet. The structure of tasks and class divisions follows the protocol established in (Ru et al. 2024). Full dataset and task details are provided in Appendix D.

Architectures For Permuted MNIST, Rotated MNIST, and Split miniImageNet, we adopt the same target network architectures as in (Ru et al. 2024), with key modifications: we introduce interval-aware variants of normalization and pooling layers, include biases, and discard the use of separate convolutional layers per task. For Split CIFAR-100, we use a streamlined interval-based version of AlexNet. Further architectural details are provided in Appendix G.

Metrics We evaluate performance using two standard continual learning metrics: Average Accuracy (AA) and Backward Transfer (BWT). AA is computed as $\frac{1}{T} \sum_{t=1}^T R_{T,t}$, where $R_{t,s}$ is the test accuracy on task s after training t tasks, where $s \leq t$. BWT is defined as $\frac{1}{T-1} \sum_{t=1}^{T-1} (R_{T,t} - R_{t,t})$, measuring the influence of learning new tasks on performance over previously learned ones. To assess continual learning performance, we evaluate accuracy on the test sets of all prior tasks.

Results Table 1 reports the AA and BWT obtained by SHIELD and several baselines after sequential learning over all tasks in the Permuted MNIST, Rotated MNIST, Split CIFAR-100, and Split miniImageNet.

On Permuted MNIST, SHIELD achieves competitive AutoAttack performance, closely matching DGP, and outperforms all baselines under PGD, FGSM, and on original samples. It is the only method with positive BWT, indicating both knowledge retention and improvement on past tasks. SHIELD_{IM} further improves PGD and clean accuracy, with a minor BWT trade-off.

On Rotated MNIST, SHIELD outperforms all baselines across all metrics, including AutoAttack, PGD, FGSM, and clean accuracy. SHIELD_{IM} enhances PGD and clean performance further, demonstrating robustness to rotation-based shifts.

On the more complex Split CIFAR-100 benchmark, SHIELD again achieves the top AA under AutoAttack and PGD. While its original sample AA and BWT are slightly below GPM and DGP, they improve with the Interval MixUp variant, confirming scalability to harder tasks while maintaining strong adversarial performance.

Table 1: AA performance after all tasks on the Permuted/Rotated MNIST, Split CIFAR-100, and Split miniImageNet. Results for SHIELD and SHIELD with Interval MixUp (SHIELD_{IM}) are averaged over 2 seeds for AutoAttack and 5 seeds for the other evaluations, except for Split miniImageNet (3 seeds, 2 for AutoAttack). Baseline results are from (Ru et al. 2024). Extended results with standard deviations are in Appendix I

Method	AutoAttack	PGD	FGSM	Original samples	
Metric	AA(%)	AA(%)	AA(%)	AA(%)	BWT
Permuted MNIST					
SGD	14.1	15.4	21.8	36.8	-0.66
SI	14.3	16.5	22.3	36.9	-0.67
A-GEM	14.1	19.7	22.9	48.4	-0.54
EWC	39.4	43.1	50.0	84.9	-0.12
GEM	12.1	75.5	72.8	96.4	-0.01
OGD	19.7	24.1	26.0	46.8	-0.57
GPM	70.4	72.9	65.7	97.2	-0.01
DGP	81.6	81.2	75.8	97.6	-0.01
SHIELD	80.91	90.11	78.87	93.58	0.02
SHIELD _{IM}	80.08	97.44	79.09	97.96	-0.05
Rotated MNIST					
SGD	14.1	9.9	20.4	32.3	-0.71
SI	13.9	15.3	20.1	33.0	-0.72
A-GEM	14.1	21.6	24.8	45.4	-0.57
EWC	45.1	49.5	46.5	80.7	-0.18
GEM	11.9	76.5	74.4	96.7	-0.01
OGD	19.7	23.8	23.8	48.0	-0.55
GPM	68.8	71.5	65.9	97.1	-0.01
DGP	81.6	82.6	78.6	98.1	-0.00
SHIELD	85.64	92.94	83.82	95.62	-0.03
SHIELD _{IM}	82.91	97.88	83.03	98.32	-0.08
Split CIFAR-100					
SGD	10.3	12.8	19.4	46.5	-0.49
SI	13.0	15.2	19.8	45.4	-0.48
A-GEM	12.6	12.9	20.7	40.6	-0.48
EWC	12.6	23.2	30.5	56.8	-0.35
GEM	21.2	19.4	47.7	60.6	-0.13
OGD	11.8	14.1	18.9	44.2	-0.50
GPM	34.4	36.6	53.7	58.2	-0.10
DGP	36.6	39.2	48.0	67.2	-0.13
SHIELD	60.91	59.77	45.37	64.24	-0.34
SHIELD _{IM}	63.08	62.39	46.48	67.45	-0.41
Split miniImageNet					
SGD	20.5	22.0	23.5	30.8	-0.24
A-GEM	19.0	19.8	21.2	29.2	-0.28
EWC	21.3	22.7	24.3	29.9	-0.25
SI	20.4	21.3	22.7	28.1	-0.27
GEM	22.3	23.8	25.4	31.8	-0.20
OGD	17.9	18.8	20.7	29.6	-0.29
GPM	26.3	27.1	28.8	36.8	-0.12
DGP	32.1	33.8	35.5	44.8	-0.05
SHIELD	56.22	56.8	53.08	59.52	-0.16
SHIELD _{IM}	57.9	58.47	54.1	62.67	-0.18

Across benchmarks, SHIELD demonstrates a strong balance between adversarial robustness and generalization. This balance is non-trivial due to the well-known trade-off: larger training ϵ improves robustness under AA and PGD, but can degrade performance on original samples due to increased regularization. SHIELD_{IM}

effectively mitigates this issue, consistently improving both adversarial and original sample AA. The relatively low FGSM results are explained by a mismatch between test-time $\varepsilon_{\text{attack}}$ and the training ε .

As shown in Table 1, on Split miniImageNet, SHIELD significantly outperforms all baselines across all metrics. While DGP and GPM reach original sample AA of 44.8% and 36.8%, respectively, SHIELD achieves 59.52%, and SHIELD_{IM} reaches 62.67%. It achieves the best AA on every task and the overall average. Forgetting (measured by BWT) is also well-controlled, with SHIELD and SHIELD_{IM} reaching -0.16 and -0.18, respectively, while achieving far higher AA.

Taken together, the results confirm that SHIELD supports robust and scalable continual learning. It maintains and improves performance over time, builds adversarially robust representations, and generalizes well across diverse tasks. Interval MixUp further improves the robustness-accuracy trade-off, making SHIELD_{IM} a practical and effective solution under adversarial threat models.

6 Conclusions

SHIELD is the first certifiably robust continual learning method, combining hypernetworks with interval arithmetic to ensure robustness across tasks. Its core, Interval MixUp, assigns smaller perturbation radii to virtual points farther from real data, tightening bounds and pushing decision boundaries away from certified regions, enhancing both robustness and accuracy, even under large perturbations and on challenging datasets.

Furthermore, SHIELD represents the first demonstrated approach to achieving substantial certified robustness in the CIL setting. This highlights the method’s ability to unify continual adaptation with formal guarantees, marking an important step toward robust lifelong learning.

Limitations While SHIELD achieves strong certified robustness and adaptability across tasks, the use of IBP, despite its computational efficiency, may lead to overly conservative (i.e., wide) interval bounds. This can affect both the certified robustness and the efficiency of the continual learner, especially in high-dimensional settings.

References

Aljundi, R.; Babiloni, F.; Elhoseiny, M.; Rohrbach, M.; and Tuytelaars, T. 2018. Memory aware synapses: Learning what (not) to forget. In *Proceedings of the European conference on computer vision (ECCV)*, 139–154.

Athalye, A.; Carlini, N.; and Wagner, D. 2018. Obfuscated gradients give a false sense of security: Circumventing defenses to adversarial examples. In *International conference on machine learning*, 274–283. PMLR.

Bagnall, A.; Bunescu, R.; and Stewart, G. 2017. Train-

ing ensembles to detect adversarial examples. *arXiv preprint arXiv:1712.04006*.

Brendel, W.; Rauber, J.; and Bethge, M. 2017. Decision-based adversarial attacks: Reliable attacks against black-box machine learning models. *arXiv preprint arXiv:1712.04248*.

Chaudhry, A.; Khan, N.; Dokania, P. K.; and Torr, P. H. S. 2020. Continual Learning in Low-rank Orthogonal Subspaces. arXiv:2010.11635.

Chen, P.-Y.; Zhang, H.; Sharma, Y.; Yi, J.; and Hsieh, C.-J. 2017. Zoo: Zeroth order optimization based black-box attacks to deep neural networks without training substitute models. In *Proceedings of the 10th ACM workshop on artificial intelligence and security*, 15–26.

Croce, F.; and Hein, M. 2020. Reliable evaluation of adversarial robustness with an ensemble of diverse parameter-free attacks. arXiv:2003.01690.

De Lange, M.; Aljundi, R.; Masana, M.; Parisot, S.; Jia, X.; Leonardis, A.; Slabaugh, G.; and Tuytelaars, T. 2021. A continual learning survey: Defying forgetting in classification tasks. *IEEE transactions on pattern analysis and machine intelligence*, 44(7): 3366–3385.

Dong, Y.; Liao, F.; Pang, T.; Su, H.; Zhu, J.; Hu, X.; and Li, J. 2018. Boosting adversarial attacks with momentum. In *Proceedings of the IEEE conference on computer vision and pattern recognition*, 9185–9193.

Dong, Y.; Pang, T.; Su, H.; and Zhu, J. 2019. Evading defenses to transferable adversarial examples by translation-invariant attacks. In *Proceedings of the IEEE/CVF conference on computer vision and pattern recognition*, 4312–4321.

Goldblum, M.; Fowl, L.; Feizi, S.; and Goldstein, T. 2020. Adversarially robust distillation. In *Proceedings of the AAAI conference on artificial intelligence*, volume 34, 3996–4003.

Goodfellow, I. J.; Shlens, J.; and Szegedy, C. 2014. Explaining and harnessing adversarial examples. *arXiv preprint arXiv:1412.6572*.

Gowal, S.; Dvijotham, K.; Stanforth, R.; Bunel, R.; Qin, C.; Uesato, J.; Arandjelovic, R.; Mann, T.; and Kohli, P. 2018. On the effectiveness of interval bound propagation for training verifiably robust models. *arXiv preprint arXiv:1810.12715*.

Ha, D.; Dai, A.; and Le, Q. V. 2016. Hypernetworks. *arXiv preprint arXiv:1609.09106*.

Hayes, T. L.; Cahill, N. D.; and Kanan, C. 2019. Memory efficient experience replay for streaming learning. In *2019 International Conference on Robotics and Automation (ICRA)*, 9769–9776. IEEE.

He, K.; Zhang, X.; Ren, S.; and Sun, J. 2016. Deep residual learning for image recognition. In *Proceedings of the IEEE conference on computer vision and pattern recognition*, 770–778.

Henning, C.; Cervera, M.; D’Angelo, F.; Von Oswald, J.; Traber, R.; Ehret, B.; Kobayashi, S.; Grewe, B. F.;

- and Sacramento, J. 2021. Posterior meta-replay for continual learning. *Advances in Neural Information Processing Systems*, 34: 14135–14149.
- Hsu, Y.-C.; Liu, Y.-C.; Ramasamy, A.; and Kira, Z. 2018. Re-evaluating continual learning scenarios: A categorization and case for strong baselines. *arXiv preprint arXiv:1810.12488*.
- Huang, L.; Joseph, A. D.; Nelson, B.; Rubinstein, B. I.; and Tygar, J. D. 2011. Adversarial machine learning. In *Proceedings of the 4th ACM workshop on Security and artificial intelligence*, 43–58.
- Jia, X.; Zhang, Y.; Wu, B.; Ma, K.; Wang, J.; and Cao, X. 2022. Las-at: adversarial training with learnable attack strategy. In *Proceedings of the IEEE/CVF conference on computer vision and pattern recognition*, 13398–13408.
- Jin, G.; Shen, S.; Zhang, D.; Dai, F.; and Zhang, Y. 2019. Ape-gan: Adversarial perturbation elimination with gan. In *ICASSP 2019-2019 IEEE International Conference on Acoustics, Speech and Signal Processing (ICASSP)*, 3842–3846. IEEE.
- Khan, H.; Shah, P. M.; Zaidi, S. F. A.; Zia, Q.; et al. 2022. Susceptibility of continual learning against adversarial attacks. *arXiv preprint arXiv:2207.05225*.
- Kirkpatrick, J.; Pascanu, R.; Rabinowitz, N.; Veness, J.; Desjardins, G.; Rusu, A. A.; Milan, K.; Quan, J.; Ramalho, T.; Grabska-Barwinska, A.; et al. 2017. Overcoming catastrophic forgetting in neural networks. *Proceedings of the national academy of sciences*, 114(13): 3521–3526.
- Krukowski, P.; Bielawska, A.; Książek, K.; Wawrzyński, P.; Batorski, P.; and Spurek, P. 2024. HyperInterval: Hypernetwork approach to training weight interval regions in continual learning. *arXiv preprint arXiv:2405.15444*.
- Książek, K.; and Spurek, P. 2023. HyperMask: Adaptive Hypernetwork-based Masks for Continual Learning. *arXiv preprint arXiv:2310.00113*.
- Li, Z.; and Hoiem, D. 2017. Learning without forgetting. *IEEE transactions on pattern analysis and machine intelligence*, 40(12): 2935–2947.
- Liu, H.; and Liu, H. 2022. Continual Learning with Recursive Gradient Optimization. *arXiv:2201.12522*.
- Lomonaco, V.; and Maltoni, D. 2017. Core50: a new dataset and benchmark for continuous object recognition. In *Conference on robot learning*, 17–26. PMLR.
- Lopez-Paz, D.; and Ranzato, M. 2017. Gradient episodic memory for continual learning. In *Proceedings of the 31st International Conference on Neural Information Processing Systems, NIPS’17*, 6470–6479. Red Hook, NY, USA: Curran Associates Inc. ISBN 9781510860964.
- Madry, A.; Makelov, A.; Schmidt, L.; Tsipras, D.; and Vladu, A. 2017. Towards deep learning models resistant to adversarial attacks. *arXiv preprint arXiv:1706.06083*.
- Mallya, A.; and Lazebnik, S. 2018. Packnet: Adding multiple tasks to a single network by iterative pruning. In *Proceedings of the IEEE conference on Computer Vision and Pattern Recognition*, 7765–7773.
- Mazur, M.; Pustelnik, L.; Knop, S.; Pagacz, P.; and Spurek, P. 2022. Target layer regularization for continual learning using Cramer-Wold distance. *Information Sciences*, 609: 1369–1380.
- McCloskey, M.; and Cohen, N. J. 1989. Catastrophic interference in connectionist networks: The sequential learning problem. In *Psychology of learning and motivation*, volume 24, 109–165. Elsevier.
- Mirman, M.; Gehr, T.; and Vechev, M. 2018. Differentiable abstract interpretation for provably robust neural networks. In *International Conference on Machine Learning*, 3578–3586. PMLR.
- Morawiecki, P.; Spurek, P.; Śmieja, M.; and Tabor, J. 2019. Fast and stable interval bounds propagation for training verifiably robust models. *arXiv preprint arXiv:1906.00628*.
- Mustafa, A.; Khan, S. H.; Hayat, M.; Goecke, R.; Shen, J.; and Shao, L. 2020. Deeply supervised discriminative learning for adversarial defense. *IEEE transactions on pattern analysis and machine intelligence*, 43(9): 3154–3166.
- Neumaier, A. 1993. *The wrapping effect, ellipsoid arithmetic, stability and confidence regions*. Springer.
- Pang, T.; Yang, X.; Dong, Y.; Su, H.; and Zhu, J. 2020. Bag of tricks for adversarial training. *arXiv preprint arXiv:2010.00467*.
- Ru, X.; Cao, X.; Liu, Z.; Moore, J. M.; Zhang, X.-Y.; Zhu, X.; Wei, W.; and Yan, G. 2024. Maintaining Adversarial Robustness in Continuous Learning. *arXiv preprint arXiv:2402.11196*.
- Rusu, A. A.; Rabinowitz, N. C.; Desjardins, G.; Soyer, H.; Kirkpatrick, J.; Kavukcuoglu, K.; Pascanu, R.; and Hadsell, R. 2016. Progressive neural networks. *arXiv preprint arXiv:1606.04671*.
- Saha, G.; Garg, I.; and Roy, K. 2021. Gradient projection memory for continual learning. *arXiv preprint arXiv:2103.09762*.
- Shi, C.; Holtz, C.; and Mishne, G. 2021. Online adversarial purification based on self-supervision. *arXiv preprint arXiv:2101.09387*.
- Su, J.; Vargas, D. V.; and Sakurai, K. 2019. One pixel attack for fooling deep neural networks. *IEEE Transactions on Evolutionary Computation*, 23(5): 828–841.
- Szegedy, C.; Zaremba, W.; Sutskever, I.; Bruna, J.; Erhan, D.; Goodfellow, I.; and Fergus, R. 2013. Intriguing properties of neural networks. *arXiv preprint arXiv:1312.6199*.
- von Oswald, J.; Henning, C.; Grewe, B. F.; and Sacramento, J. 2019. Continual learning with hypernetworks. In *International Conference on Learning Representations*.

Wang, L.; Zhang, X.; Su, H.; and Zhu, J. 2024. A comprehensive survey of continual learning: Theory, method and application. *IEEE Transactions on Pattern Analysis and Machine Intelligence*.

Wortsman, M.; Ramanujan, V.; Liu, R.; Kembhavi, A.; Rastegari, M.; Yosinski, J.; and Farhadi, A. 2020. Supermasks in superposition. *Advances in Neural Information Processing Systems*, 33: 15173–15184.

Xie, C.; Wang, J.; Zhang, Z.; Ren, Z.; and Yuille, A. 2017. Mitigating adversarial effects through randomization. *arXiv preprint arXiv:1711.01991*.

Yang, Z.; Xu, Z.; Zhang, J.; Hartley, R.; and Tu, P. 2022. Adaptive test-time defense with the manifold hypothesis. *arXiv preprint arXiv:2210.14404*, 3.

Zenke, F.; Poole, B.; and Ganguli, S. 2017. Continual learning through synaptic intelligence. In *International conference on machine learning*, 3987–3995. PMLR.

Zhang, H.; Cisse, M.; Dauphin, Y. N.; and Lopez-Paz, D. 2018a. mixup: Beyond Empirical Risk Minimization. *arXiv:1710.09412*.

Zhang, H.; Weng, T.-W.; Chen, P.-Y.; Hsieh, C.-J.; and Daniel, L. 2018b. Efficient Neural Network Robustness Certification with General Activation Functions. *arXiv:1811.00866*.

Zhou, Y.; and Hua, Z. 2024. Defense without forgetting: Continual adversarial defense with anisotropic & isotropic pseudo replay. In *Proceedings of the IEEE/CVF Conference on Computer Vision and Pattern Recognition*, 24263–24272.

Zhu, J.; Yao, J.; Han, B.; Zhang, J.; Liu, T.; Niu, G.; Zhou, J.; Xu, J.; and Yang, H. 2021. Reliable adversarial distillation with unreliable teachers. *arXiv preprint arXiv:2106.04928*.

A Extended related works

This work introduces a novel synthesis of two previously disjoint research areas in deep learning: continual learning and adversarial robustness. Since existing literature rarely addresses their intersection, we organize the related work section around both foundations to highlight the unique contributions of our method.

Adversarial Attack Adversarial attacks on deep neural networks are typically categorized as white-box or black-box, depending on the attacker’s access to the target model. In white-box settings, the adversary fully knows the model, including its architecture, parameters, and gradients. Prominent white-box attacks include gradient-based methods such as FGSM (Goodfellow, Shlens, and Szegedy 2014), BIM (Huang et al. 2011), MIM (Dong et al. 2018), PGD (Madry et al. 2017), and AutoAttack (De Lange et al. 2021), as well as optimization-based approaches like the OnePixel (Su, Vargas, and Sakurai 2019).

In black-box settings, attackers have limited access to the model and must rely on indirect signals. Some approaches use confidence scores to estimate gradients,

such as zoo (Chen et al. 2017), while others operate with only the predicted label, as seen in decision-based methods like the Boundary Attack (Brendel, Rauber, and Bethge 2017). Another strategy involves crafting adversarial examples on a surrogate model and transferring them to the target model, exploiting the cross-model transferability of adversarial perturbations (Dong et al. 2018, 2019).

Simultaneously with adversarial attack techniques, there are many defence algorithms. Early adversarial defenses relied on heuristics such as input transformations (Xie et al. 2017), model ensembles (Bagnall, Bunescu, and Stewart 2017), and denoisers (Jin et al. 2019), but many were later found to rely on obfuscated gradients (Athalye, Carlini, and Wagner 2018). More robust approaches like adversarial training (AT) (Goodfellow, Shlens, and Szegedy 2014; Jia et al. 2022) and defensive distillation (Goldblum et al. 2020; Zhu et al. 2021) have become dominant. Recent work has enhanced AT with learnable strategies (Jia et al. 2022), feature perturbation (Mustafa et al. 2020), and optimization techniques (Pang et al. 2020). However, the above models are typically static and struggle against evolving attack sequences. Test-Time Adaptation Defense (Shi, Holtz, and Mishne 2021; Yang et al. 2022) addresses adaptation to new attacks but neglects previous ones.

Most existing methods aim to improve adversarial robustness, but they do so without providing formal guarantees. Interval Bound Propagation (IBP) (Gowal et al. 2018; Mirman, Gehr, and Vechev 2018) offers a principled alternative by using interval arithmetic to train models that are provably robust against adversarial attacks. These methods enforce that the model classifies all points within a specified perturbation region (typically a ball in ℓ_∞) correctly, by optimizing a worst-case cross-entropy loss.

Continual Learning Continual learning methods are often grouped into architectural, rehearsal, and regularization-based strategies (Hsu et al. 2018). Architectural approaches like Progressive Neural Networks (Rusu et al. 2016) and CopyWeights with Reinit (Lomonaco and Maltoni 2017) prevent forgetting by expanding or modifying network structures. Further developments reuse a fixed architecture with iterative pruning, such as PackNet (Mallya and Lazebnik 2018) or Supermasks (Wortsman et al. 2020). Rehearsal-based methods, such as the buffer strategy in (Hayes, Cahill, and Kanan 2019), retain selected past examples, while pseudo-rehearsal approaches train generative models to replay prior data (Mazur et al. 2022). Regularization-based techniques like EWC (Kirkpatrick et al. 2017), SI (Zenke, Poole, and Ganguli 2017), LwF (Li and Hoiem 2017), and MAS (Aljundi et al. 2018) constrain parameter updates based on past task importance, often using the Fisher Information Matrix or similar metrics.

Hypernetworks, introduced in (Ha, Dai, and Le 2016), are defined as neural models that generate

weights for a separate target network that solves a specific task. The authors aim to reduce the number of trainable parameters by designing a hypernetwork that often has fewer parameters than the target network. In continual learning, hypernetworks can directly generate individual weights for subsequent continual learning tasks, like in HNET (von Oswald et al. 2019). Then, HNET was extended with a probabilistic approach called posterior meta-replay (Henning et al. 2021). In HyperMask (Książek and Spurek 2023), the authors used the lottery ticket hypothesis to produce task-specific masks for the trainable or fixed target model. In (Krukowski et al. 2024), the authors employ interval arithmetic on weights to regularize the target model. These methods are positioned between those based on architecture and those focused on regularization.

The above concepts have many different modifications and upgrades (Wang et al. 2024). But the adversarial robustness of continual learning problems is unexplored in the literature. AIR (Zhou and Hua 2024) introduced the first framework for continual adversarial defense, addressing robustness against evolving attack sequences. The method leverages unsupervised data augmentation to enhance general robustness in a task-agnostic manner. While innovative, AIR is limited in scalability, having been evaluated on only two to three defense tasks, raising concerns about its effectiveness in longer, continual settings.

Alternatively, the study on Double Gradient Projection (DGP) (Ru et al. 2024) highlights that this technique is notably more resilient to adversarial attacks compared to traditional continual learning approaches such as GEM (Lopez-Paz and Ranzato 2017) and GPM (Saha, Garg, and Roy 2021). DGP enhances adversarial robustness by projecting gradients orthogonally concerning a critical subspace before updating weights, thus maintaining the prior gradient smoothness from earlier samples. Furthermore, (Khan et al. 2022) examines the resistance of current models against adversarial assaults. These methodologies enhance the robustness of continual learning, yet they have several significant limitations. Firstly, such approaches are restricted to several subsequent tasks and do not give strict guarantees.

B MixUp

Definition B.1 (MixUp). Given two training examples (x_i, y_i) and (x_j, y_j) drawn independently from the data distribution, MixUp constructs a new virtual training example (\tilde{x}, \tilde{y}) as:

$$\tilde{x} = \lambda x_i + (1 - \lambda)x_j, \quad (19)$$

$$\tilde{y} = \lambda y_i + (1 - \lambda)y_j, \quad (20)$$

where $\lambda \in [0, 1]$ is sampled from the Beta distribution, $\lambda \sim \text{Beta}(\alpha, \alpha)$, with a fixed hyperparameter $\alpha > 0$.

Here, $y_i, y_j \in \mathbb{R}^M$ are typically one-hot encoded class labels, so the mixed label \tilde{y} becomes a soft target, a

convex combination of label vectors. To train a model with such soft labels, the loss function must support probabilistic targets. A common choice is the soft-label cross-entropy loss:

$$\mathcal{L}(\tilde{y}, \hat{y}) = - \sum_{k=1}^M \tilde{y}_k \log \hat{y}_k, \quad (21)$$

where \hat{y} denotes the model’s predicted probability distribution over classes. This formulation encourages linear behavior between training examples, often improving generalization and calibration.

C Interval Neural Network Layers

The implementation of linear and convolutional layers in the interval version is straightforward and follows the approach described in the main part. However, implementing other interval layers requires more care and is not as trivial.

Interval Batch Normalization Batch normalization in the interval version is more involved. Instead of simply normalizing the lower and upper bounds separately, we first concatenate the lower and upper bounds into a single tensor. We then compute the batch statistics, mean, and variance, over this combined tensor, capturing the distribution of the entire interval. Using these statistics, we apply the standard batch normalization transformation.

More concretely, given pre-activation interval bounds $[\underline{x}, \bar{x}]$, we form the concatenated tensor:

$$X_{\text{concat}} = [\underline{x}, \bar{x}], \quad (22)$$

and compute the expected mean μ and variance σ^2 over X_{concat} . We then normalize and scale the interval bounds as follows:

$$\left[\frac{\underline{x} - \mu}{\sqrt{\sigma^2 + \varepsilon}}, \frac{\bar{x} - \mu}{\sqrt{\sigma^2 + \varepsilon}} \right], \quad (23)$$

followed by the affine transformation with learned parameters γ (scale) and β (shift):

$$\gamma \cdot \left[\frac{\underline{x} - \mu}{\sqrt{\sigma^2 + \varepsilon}}, \frac{\bar{x} - \mu}{\sqrt{\sigma^2 + \varepsilon}} \right] + \beta. \quad (24)$$

We add a small positive constant ε to the denominator to ensure numerical stability. Special attention is required to handle the sign of γ correctly to maintain valid lower and upper bounds. If the sign of γ is negative, the lower and upper bounds must be swapped after scaling to preserve correct interval ordering.

Interval Pooling Layers Pooling operations can be extended to the interval version by applying them separately to the lower and upper bounds of each input element.

For max pooling, given a set of input intervals $\{[\underline{x}_i, \bar{x}_i]\}_{i=1}^n$, the output interval is computed as:

$$\text{MaxPool}_{\text{inf}} = \max_{1 \leq i \leq n} \underline{x}_i, \quad (25)$$

$$\text{MaxPool}_{\text{sup}} = \max_{1 \leq i \leq n} \bar{x}_i, \quad (26)$$

and the resulting output interval is $[\text{MaxPool}_{\text{inf}}, \text{MaxPool}_{\text{sup}}]$.

For average pooling, the interval is computed by averaging the bounds independently:

$$\text{AvgPool}_{\text{inf}} = \frac{1}{n} \sum_{i=1}^n \underline{x}_i, \quad (27)$$

$$\text{AvgPool}_{\text{sup}} = \frac{1}{n} \sum_{i=1}^n \bar{x}_i, \quad (28)$$

so that the final interval is $[\text{AvgPool}_{\text{inf}}, \text{AvgPool}_{\text{sup}}]$.

Average pooling often produces tighter and more stable bounds, and is therefore preferred in interval-based analysis such as IBP.

D Benchmark Datasets

Permuted MNIST introduces a different fixed pixel permutation for each task, applied to the original MNIST images. Rotated MNIST, on the other hand, creates tasks by rotating the digits by varying angles. These two datasets are widely used in the continual learning literature as synthetic benchmarks derived from MNIST (Goodfellow, Shlens, and Szegedy 2014; Liu and Liu 2022). Split CIFAR-100 (Zenke, Poole, and Ganguli 2017) is constructed by randomly partitioning the 100 classes of the CIFAR-100 dataset into 10 mutually exclusive groups, with each group forming a separate classification task of 10 classes. Similarly, Split miniImageNet is generated by selecting a subset of the original ImageNet dataset (Chaudhry et al. 2020) and dividing it into 20 distinct groups, each containing 5 unique classes. For both Split CIFAR-100 and Split miniImageNet, each class appears in only one group, ensuring no class overlap between tasks. This design allows each subset to be treated as an independent classification task, resulting in a sequence of tasks for continual learning. To match the setup of Split miniImageNet presented in (Ru et al. 2024), we split Split miniImageNet as described; however, we use only the first ten tasks. Therefore, we have 10 tasks, each with 5 classes.

E Discussion on Learnable Number of Parameters Used in SHIELD

Since we employ hypernetworks to generate the weights of the target network, the total number of learnable parameters is typically higher than that of baseline architectures. However, we demonstrate that it is possible to significantly reduce this parameter count, bringing it in line with standard models, while still achieving state-of-the-art performance. Importantly, the number of parameters in the target network remains comparable to, or even smaller than, those of the baseline models; the additional overhead stems solely from the hypernetwork. The Interval MixUp technique is also not used in this experiment.

For the Permuted MNIST dataset, we reduce the number of learnable parameters to match the budget

used in (Ru et al. 2024) by employing a hypernetwork composed of a two-layer MLP with hidden dimensions 100 and 50, and an embedding size of 96. The target network is a two-layer MLP with 50 neurons per layer. For the Rotated MNIST dataset, we adopt the same architecture but reduce the embedding size to 24 to further minimize the parameter count. We use $\varepsilon = \frac{25}{255}$ for both Permuted MNIST and Rotated MNIST during training.

For the Split CIFAR-100 dataset, again we align with the parameter budget from (Ru et al. 2024) by using an embedding size of 512 and a hypernetwork consisting of a two-layer MLP with 200 and 50 hidden units, respectively. Additionally, we simplify the target AlexNet architecture by removing two fully connected layers, applying a 4×4 average pooling operation after the final convolutional layer in place of the max pooling, and reducing the hidden dimension of the last linear layer to 100. For Split CIFAR-100, we use $\varepsilon = \frac{2}{255}$ during training.

The total number of learnable parameters used in each configuration is reported in Table 2. Furthermore, we adopt the same FGSM, PGD, and AutoAttack settings as described in the main paper.

Tables 3, 4, and 5 present the AA of SHIELD and several baselines after learning all tasks sequentially. The results include performance under three adversarial attacks (AutoAttack, PGD, FGSM) and on original clean data.

On the Permuted MNIST benchmark (Table 3), SHIELD delivers the strongest adversarial robustness among all compared methods. It surpasses prior approaches under all attack settings, including AutoAttack, PGD, and FGSM, establishing itself as the most resilient model to adversarial perturbations in this setting. While a few baselines, particularly DGP and GPM, achieve higher clean accuracy, their robustness drops notably under stronger attacks. In contrast, SHIELD maintains both high robustness and solid performance on clean samples, without relying on overly large architectures or task-specific replay. This highlights the method’s ability to generalize under distribution shifts and adversarial pressure, a balance that remains a major challenge in continual learning.

On Rotated MNIST (Table 4), SHIELD sets a new state-of-the-art across all evaluated attacks. It achieves the highest Average Accuracy (AA) under AutoAttack (90.36%), PGD (92.76%), and FGSM (82.21%), outperforming strong baselines like DGP and GPM by a significant margin. Moreover, SHIELD not only maintains robust performance but also retains high AA (93.12%) on original samples, closely matching the top-performing baselines in that category.

On the more complex Split CIFAR-100 benchmark (Table 5), SHIELD once again delivers the strongest performance under adversarial attacks. It outperforms all baselines by a wide margin in both AutoAttack and PGD evaluations, achieving 54.55% and 54.53% AA, respectively, substantially ahead of the next best method,

Table 2: Comparison of learnable parameters (in millions) between our method and the baseline methods from (Ru et al. 2024), which we refer to simply as "Baseline". Our reduced version achieves comparable or better performance with a similar or smaller number of parameters.

Method	Permuted MNIST	Rotated MNIST	Split CIFAR-100
Baseline	2M	2M	5.5M
SHIELD	2.8M	2.8M	5.6M

Table 3: Comparison of AA after completing all tasks on the Permuted MNIST dataset. AA results for SHIELD are averaged over 2 seeds for AutoAttack and 5 seeds for all other evaluations.

Method	Permuted MNIST			
	AutoAttack	PGD	FGSM	Original samples
	AA(%)	AA(%)	AA(%)	AA(%)
SGD	14.1	15.4	21.8	36.8
SI	14.3	16.5	22.3	36.9
A-GEM	14.1	19.7	22.9	48.4
EWC	39.4	43.1	50.0	84.9
GEM	12.1	75.5	72.8	96.4
OGD	19.7	24.1	26.0	46.8
GPM	70.4	72.9	65.7	97.2
DGP	81.6	81.2	75.8	97.6
SHIELD	88.43 ± 0.35	90.47 ± 1.36	79.6 ± 1.34	90.71 ± 1.8

DGP. While some baselines achieve slightly better AA on original samples, they fall short under adversarial threat models. In contrast, SHIELD consistently balances robustness and plasticity, confirming its capacity to learn durable representations without catastrophic forgetting, even in challenging continual learning settings.

While SHIELD does not achieve the highest AA on original samples in this setup, it remains competitive with top methods like DGP. We emphasize that Interval MixUp was not used; our goal is to show that SHIELD performs well even without it and with a smaller target network architecture. The slight drop in clean accuracy stems from two deliberate choices: (1) SHIELD is trained using a relatively small target network architecture, and (2) training with stronger adversarial perturbations, which often lowers clean accuracy but improves robustness. This trade-off allows SHIELD to strike a strong balance between robustness and performance, making it a reliable option for adversarially robust continual learning.

F Selected Hyperparameters

For the Split CIFAR-100 experiments, we used an AlexNet-based target network along with a hypernetwork comprising two hidden layers of 100 and 50 neurons, respectively. The embedding size was set to 512, with a batch size of 32 and a learning rate of 0.001. The hypernetwork used a regularization coefficient $\beta = 0.01$, and training was performed with an ℓ_∞ perturbation of $\varepsilon = 0.005$. The optimizer was Adam, and no data augmentation was used. Training was conducted for 200 epochs with ReLU activation in both the target and

hypernetwork. We applied a learning rate scheduler: ReduceLROnPlateau with monitoring set to the maximum validation accuracy, reduction factor $\sqrt{0.1}$, patience of 5 epochs, minimum learning rate of 5×10^{-7} , and no cooldown. Batch normalization was enabled throughout. When Interval MixUp is applied, we sample the mixing coefficient from a Beta distribution with parameter $\alpha = 0.3$.

For the Permuted MNIST task, we employed a 2-layer MLP with 256 neurons per layer in the target network and 100 neurons per layer in the hypernetwork. The embedding size was 24, the batch size was 128, and the learning rate was 0.001. We used $\beta = 0.001$ and performed training with $\varepsilon = 0.01$. For the Rotated MNIST experiments, the setup mirrored that of Permuted MNIST but used an embedding size of 96. Training on Permuted MNIST and Rotated MNIST was conducted for 5000 iterations. When using Interval MixUp, we set the Beta distribution parameter to $\alpha = 0.1$.

In the Split miniImageNet experiments, we used a ResNet-18 target network and a hypernetwork with two hidden layers of 100 and 50 neurons, respectively. The embedding dimension was 128, with a batch size of 16 and a learning rate of 0.001. We trained using the Adam optimizer for 50 epochs, applying ReLU activations and enabling batch normalization throughout. The hypernetwork was regularized with $\beta = 0.01$, and training included an ℓ_∞ perturbation of $\varepsilon = \frac{2}{255}$. No data augmentation was used. The learning rate scheduler matched that of the Split CIFAR-100 setup. When Interval MixUp was used, mixing coefficients were drawn from a Beta distribution with $\alpha = 0.2$.

Model selection was based on the best validation loss.

Table 4: Comparison of AA after completing all tasks on the Rotated MNIST dataset. AA results for SHIELD are averaged over 2 seeds for AutoAttack and 5 seeds for all other evaluations.

Method	Rotated MNIST			
	AutoAttack	PGD	FGSM	Original samples
	AA(%)	AA(%)	AA(%)	AA(%)
SGD	14.1	9.9	20.4	32.3
SI	13.9	15.3	20.1	33.0
A-GEM	14.1	21.6	24.8	45.4
EWC	45.1	49.5	46.5	80.7
GEM	11.9	76.5	74.4	96.7
OGD	19.7	23.8	23.8	48.0
GPM	68.8	71.5	65.9	97.1
DGP	81.6	82.6	78.6	98.1
SHIELD	90.36 ± 0.1	92.76 ± 0.22	82.21 ± 0.43	93.12 ± 0.22

Table 5: Comparison of AA after completing all tasks on the Split CIFAR-100 dataset. AA results for SHIELD are averaged over 2 seeds for AutoAttack and 5 seeds for all other evaluations.

Method	Split CIFAR-100			
	AutoAttack	PGD	FGSM	Original samples
	AA(%)	AA(%)	AA(%)	AA(%)
SGD	10.3	12.8	19.4	46.5
SI	13.0	15.2	19.8	45.4
A-GEM	12.6	12.9	20.7	40.6
EWC	12.6	23.2	30.5	56.8
GEM	21.2	19.4	47.7	60.6
OGD	11.8	14.1	18.9	44.2
GPM	34.4	36.6	53.7	58.2
DGP	36.6	39.2	48.0	67.2
SHIELD	54.55 ± 0.42	54.53 ± 0.48	47.71 ± 0.86	59.36 ± 1.11

The optimizer across all experiments was Adam, and ReLU was used as the activation function throughout. In all cases, the same adversarial attack settings were used as in (Ru et al. 2024), except that the number of attack iterations for PGD was not specified in that work; we defaulted to 100 iterations for consistency across evaluations. For AutoAttack, we used the standard version with default parameters as suggested by the authors in (Croce and Hein 2020).

Experiments were conducted on NVIDIA RTX 4090 and A100 GPUs. All software and package versions are listed in the README file in our code repository.

G Training Details

To identify the most effective configuration for each dataset, we conducted an extensive grid search over key hyperparameters, evaluating combinations to maximize validation performance. Below we summarize the search spaces used for each dataset.

Permuted MNIST For the Permuted MNIST dataset, the grid search was performed using a 2-layer MLP with 256 neurons per layer in the target network. As a hypernetwork, we used an MLP, with architecture

defined by the hypernetwork hidden layers parameter. The following hyperparameters were explored:

- Embedding sizes: 24, 48, 96
- Learning rate: 0.001
- Batch sizes: 64, 128
- Regularization coefficients β : 0.0005, 0.001, 0.005, 0.01, 0.05
- Perturbation sizes ϵ : $\frac{2}{255}$, $\frac{20}{255}$, $\frac{25}{255}$, 0.01
- Hypernetwork hidden layers (MLP): [100, 50], [200, 50], [100, 100]
- Number of training iterations: 5000
- Number of validation samples per class in each task: 500
- Beta distribution hyperparameters (α): 0.01, 0.1, 0.2, 0.3, 0.4, 0.5

Rotated MNIST We use the same grid search as for the Permuted MNIST dataset.

Split CIFAR-100 For the Split CIFAR-100 dataset, the grid search was conducted using AlexNet as the target network and an MLP-based hypernetwork. Batch normalization was enabled, and data augmentation was

disabled. The full hyperparameter search space included:

- Embedding sizes: 128, 256, 512
- Learning rate: 0.001
- Batch sizes: 32, 64
- Regularization coefficients β : 0.01, 0.05, 0.1
- Perturbation sizes ε : $\frac{2}{255}$, $\frac{4}{255}$, 0.005, 0.01
- Hypernetwork hidden layers (MLP): [200, 50], [100, 50], [100, 100], [100], [200]
- Number of training epochs: 200
- Number of validation samples per class in each task: 500
- Beta distribution hyperparameters (α): α : 0.01, 0.1, 0.2, 0.3, 0.4, 0.5

Split miniImageNet For the Split miniImageNet dataset, the grid search was conducted using ResNet-18 as the target network and an MLP-based hypernetwork. Batch normalization was enabled, and data augmentation was disabled. The full hyperparameter search space included:

- Embedding sizes: 96, 128, 256
- Learning rate: 0.001
- Batch size: 16
- Regularization coefficients β : 0.01, 0.05
- Perturbation sizes ε : $\frac{1}{255}$, $\frac{2}{255}$, $\frac{4}{255}$
- Hypernetwork hidden layers (MLP): [200, 50], [100, 50], [100]
- Number of training epochs: 50
- Number of validation samples per class in each task: 250
- Beta distribution hyperparameters (α): α : 0.01, 0.1, 0.2, 0.3, 0.4, 0.5

The Adam optimizer was used across all tasks. These grid searches enabled a systematic selection of optimal configurations for each dataset.

Interval Bound Propagation Training Details

Training with overly wide intervals can destabilize the learning process, especially in the early stages. To mitigate this, we begin training with $\kappa = 1$, placing full emphasis on the standard classification loss. As training progresses, the weight on the interval bound loss increases gradually, reaching $\kappa = 0.5$ by the midpoint of training. Simultaneously, we initialize the perturbation radius at $\varepsilon = 0$ and linearly increase it during the first half of training, so that it reaches the target value at the midpoint. Both κ and ε remain fixed for the remainder of training.

Formally, let E be the total number of training iterations per task, and denote by κ_i and ε_i the values of κ and ε at iteration $i \in \{1, \dots, E\}$. We define their

schedules as:

$$\kappa_i = \max\left\{\frac{1}{2}, 1 - \frac{i}{2E}\right\} \quad (29)$$

$$\varepsilon_i = \begin{cases} \frac{2i-\varepsilon}{E} & \text{if } i \leq \lfloor \frac{E}{2} \rfloor, \\ \varepsilon & \text{otherwise.} \end{cases} \quad (30)$$

Architecture Details In the main part of the paper, we use the same base architecture across Permuted MNIST, Rotated MNIST, and Split-miniImageNet. For the Split CIFAR-100, we adopt a streamlined variant of AlexNet to meet the capacity and efficiency requirements of hypernetwork-based training. Specifically, we remove dropout, include biases, and replace standard batch normalization layers with interval-aware variants. The classifier comprises two fully connected layers with 100 units each. To improve numerical stability during IBP, we replace max pooling with average pooling. Additionally, a 4×4 average pooling layer is applied after the final convolutional layer to reduce dimensionality.

This lightweight adaptation of AlexNet ensures that the target network remains compact, which is critical for training efficiency when its parameters are generated dynamically by a hypernetwork. Importantly, unlike (Ru et al. 2024), we do not allocate separate convolutional layers for each task; our model maintains a single shared architecture across tasks. Further architectural details and hyperparameter choices are discussed in Appendix Section G. A shared MLP hypernetwork is used across all datasets.

H Ablation Study

Alternative Epsilon Decay Rate Functions in Interval MixUp

In this subsection, we investigate how different epsilon decay rates affect the training of SHIELD. In the paper, we employ a linear decay schedule. However, it is important to examine whether alternative decay strategies lead to different training behaviors. To this end, we additionally consider quadratic, logarithmic, and cosine decay functions. The corresponding plots of these decay schedules are shown in Figure 4.

Figure 5 presents the AA over time for various decay rate strategies across three continual learning benchmarks: Permuted MNIST, Split CIFAR-100, and Split miniImageNet. The top row shows AA, computed as the mean accuracy over all tasks seen so far, immediately after learning each task. The bottom row shows final AA, calculated as the average accuracy on all tasks after the final task is learned.

Across all datasets, linear and logarithmic decay rate schedules demonstrate stable and competitive performance throughout training. In contrast, cosine and quadratic functions result in noticeably unstable and degraded accuracy, particularly evident in later tasks (such as the 6th task of Split CIFAR-100 and Split miniImageNet). This instability may be attributed to the more abrupt fluctuations of cosine and quadratic

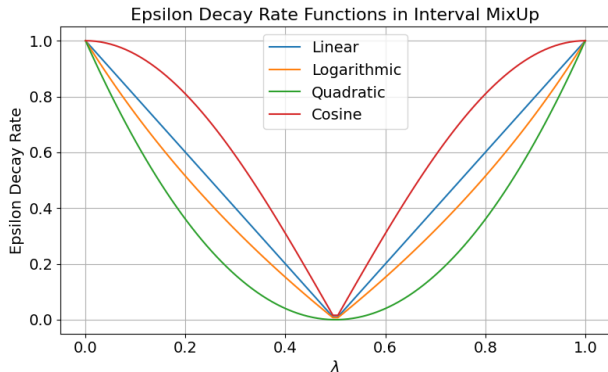


Figure 4: Comparison of different epsilon decay rates used in Interval MixUp.

schedules (Figure 4). These findings suggest that decay strategies, such as linear or logarithmic, better support robust learning in adversarial continual learning scenarios.

Table 6: Comparison of AA after completing all tasks on the Permuted MNIST dataset. AA results for different scheduling strategies (linear, quadratic, log, and cos) were calculated for a single seed.

Schedule	Permuted MNIST				
	AutoAttack AA(%)	PGD AA(%)	FGSM AA(%)	Original samples AA(%)	BWT
Linear	80.53	97.48	79.4	98.01	0.002
Quadratic	80.45	97.64	79.51	98.16	0.001
Log	80.38	97.44	79.67	97.98	-0.03
Cos	81.44	97.4	80.1	97.92	-0.05

Table 7: Comparison of AA after completing all tasks on the Split CIFAR-100 dataset. AA results for different scheduling strategies (linear, quadratic, log, and cos) were calculated for a single seed.

Schedule	Split CIFAR-100				
	AutoAttack AA(%)	PGD AA(%)	FGSM AA(%)	Original samples AA(%)	BWT
Linear	63.89	62.9	46.99	66.97	-0.22
Quadratic	63.14	62.58	46.72	67.6	-0.27
Log	62.91	62.1	46.75	67.07	-0.68
Cos	58.87	57.72	42.91	62.44	-5.29

We evaluate the performance of SHIELD trained using linear, quadratic, logarithmic, and cosine epsilon decay rate schedules in the context of adversarial attacks. The results are presented in Figures 6, 7, and 8. The attacks used are the same as those described in the main paper. On Permuted MNIST, the results are nearly identical across all schedules. However, for Split CIFAR-100 and Split miniImageNet, the linear decay strategy performs the best. In this experiment, we used the best hyperparameters identified for the linear strat-

Table 8: Comparison of AA after completing all tasks on the Split miniImageNet dataset. AA results for different scheduling strategies (linear, quadratic, log, and cos) were calculated for a single seed.

Schedule	Split miniImageNet				
	AutoAttack AA(%)	PGD AA(%)	FGSM AA(%)	Original samples AA(%)	BWT
Linear	60.08	60.32	56.16	64.72	-0.13
Quadratic	59.2	51.36	46.92	55.2	-7.33
Log	55.72	55.64	51.64	59.84	-2.09
Cos	55.52	55.84	51.88	60.2	-3.51

egy in the main paper, so it is possible that further grid search for the other schedules could yield improved results.

Impact of FGSM Perturbation Size on Average Accuracy

In Figure 6, we show the effect of FGSM attacks with varying ϵ_{attack} values on the AA metric for our method and for HNET. The results indicate that HNET is substantially more vulnerable to adversarial perturbations, with a steep drop in AA on Split CIFAR-100 and Split miniImageNet, even under small ϵ_{attack} values. For each subfigure in Figure 6, we evaluate our models using 10 FGSM attack strengths, with ϵ_{attack} values evenly spaced from 0 up to twice the ϵ (perturbation value used in the training process) used during training. This setup allows us to assess how well the models generalize robustness beyond the training-time perturbation level. The optimal ϵ values used are those identified in Section F.

Impact of PGD Iterations on Average Accuracy

In Figure 7, we present the effect of PGD attacks with an increasing number of steps on the AA metric for SHIELD and HNET. Across all evaluated datasets, SHIELD consistently achieves higher initial accuracy when subjected to no attack or only a few PGD steps. Both SHIELD and HNET exhibit a noticeable drop in AA within the first 10 to 25 steps; however, their performance then stabilizes, demonstrating resilience to stronger iterative attacks.

For each subfigure in Figure 7, we evaluate both models across 10 PGD configurations, with the number of attack steps evenly spaced from 0 to 200. The remaining PGD hyperparameters (e.g., step size, ϵ_{attack}) are kept identical to those used in the main experiments. This extended evaluation allows us to assess model robustness across a broader attack range than previously reported. As before, we use the best-performing hyperparameters identified in Section F.

These results further confirm that SHIELD provides stronger and more stable adversarial robustness, particularly under longer and more aggressive PGD attacks.

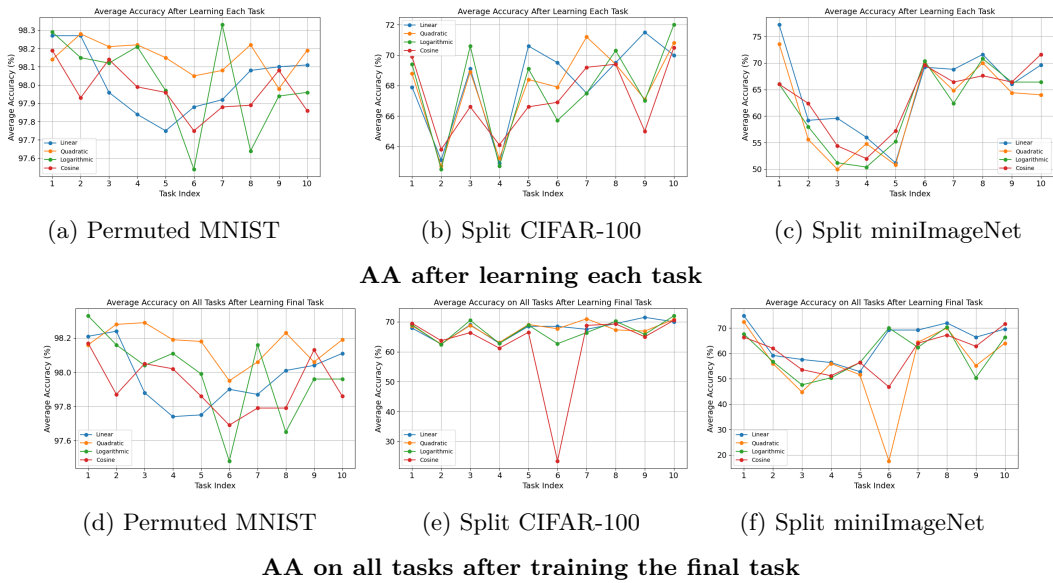


Figure 5: Comparison of results for different epsilon decay rates across (a) Permuted MNIST, (b) Split CIFAR-100, and (c) Split miniImageNet. Top row: AA measured immediately after learning each task. Bottom row: AA evaluated on all tasks after completing the final task.

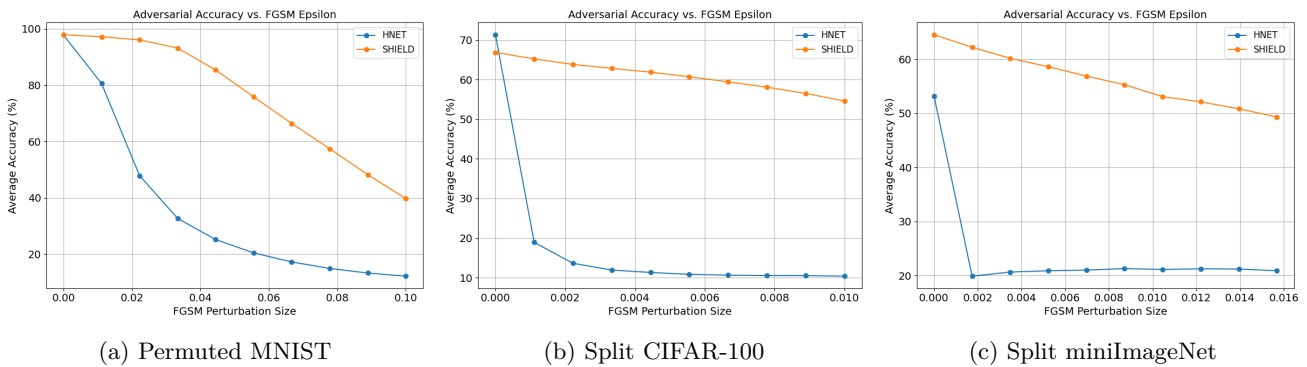


Figure 6: AA of SHIELD and HNET under FGSM attacks with increasing perturbation sizes, evaluated on models trained on Permuted MNIST (Figure 6a), Split CIFAR-100 (Figure 6b), and Split miniImageNet (Figure 6c).

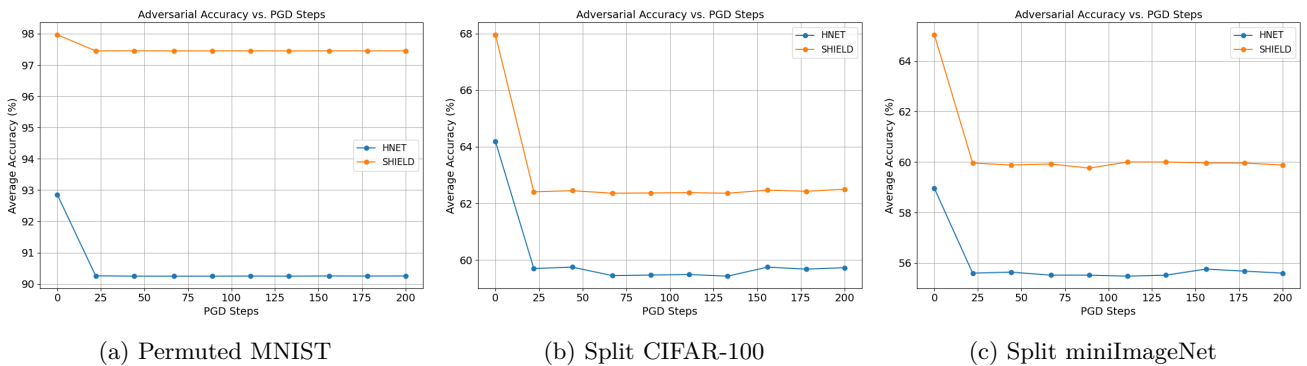
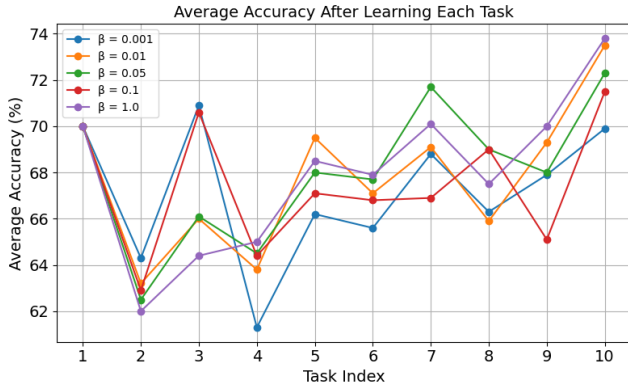


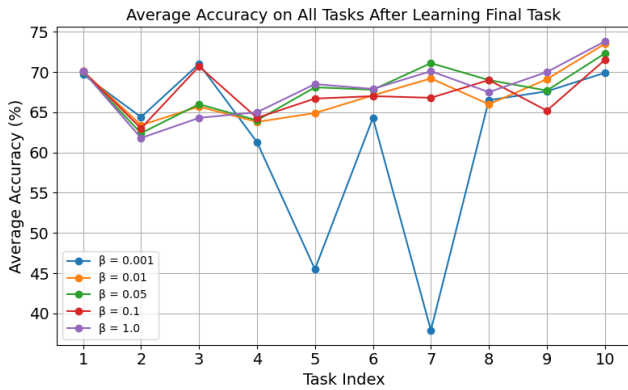
Figure 7: AA of SHIELD and HNET under PGD attacks with increasing number of gradient steps, evaluated on models trained on Permuted MNIST (Figure 7a), Split CIFAR-100 (Figure 7b), and Split miniImageNet (Figure 7c).

Impact of β Parameter Selection on Training Process of SHIELD

We evaluate the ability of SHIELD to retain knowledge across tasks, which is controlled by the hyperparameter β . In Figure 8, we present AA curves obtained by training the model with optimal hyperparameters while varying β . The results show that β values of 0.01 and 1.0 yield the best performance, ensuring stable predictions and minimal forgetting. In contrast, a small value of $\beta = 0.001$ leads to significant forgetting, particularly on the 5th and 6th tasks, after learning the final task.



(a) AA calculated directly after learning each task



(b) AA calculated after the final task

Figure 8: Comparison of AA curves for varying β values, which control hypernetwork regularization strength in SHIELD

Performance of SHIELD on TinyImageNet dataset

We assess the scalability of SHIELD on a more challenging benchmark involving a larger number of tasks. Specifically, we use TinyImageNet, a subset of ImageNet, consisting of 200 classes, each with 500 training images and 50 validation images at a resolution of 64×64 pixels. To construct the benchmark, we define 40 tasks, each composed of 5 randomly selected, non-overlapping classes. This setup allows us to evaluate

SHIELD’s performance under increased task complexity and class diversity.

We compare the robustness of SHIELD with the traditional HNET approach (von Oswald et al. 2019) under three adversarial attacks: FGSM, PGD, and AutoAttack. Both models are trained specifically on TinyImageNet. For FGSM, we set the attack strength to $\epsilon_{\text{attack}} = \frac{4}{255}$. For PGD and AutoAttack, we use $\epsilon_{\text{attack}} = \frac{2}{255}$, with a PGD step size of $\delta = \frac{4}{255}$ and 100 iterations. The AutoAttack configuration is the same as used in the main experiments of the paper.

We use ResNet-18 as the target network. The hypernetwork is implemented as a multilayer perceptron (MLP) with a single hidden layer of 100 neurons and an embedding size of 48. Results are reported using a fixed random seed set to 1, shared across both models. We train both architectures for 50 epochs using the Adam optimizer, a learning rate of 0.001, and a batch size of 128. The same learning rate scheduler as in the Split CIFAR-100 experiments is applied. We set $\beta = 0.05$. For SHIELD, we use $\epsilon = 0.005$ during training and apply Interval MixUp.

Table 9: Comparison of AA after completing all tasks on the TinyImageNet dataset.

Method	AutoAttack	PGD	FGSM	Original samples
HNET	46.37	45.3	49.17	63.83
SHIELD	51.78	52.83	52.36	64.33

From Table 9, we observe that even on a challenging dataset like TinyImageNet, our model achieves high AA on original (non-adversarial) test samples while also maintaining robustness against adversarial attacks. While HNET achieves competitive results, our method performs slightly better, especially under adversarial conditions.

I Extended Results from Main Paper

In this section, we extend results from Table 1 to attach standard deviations. We present extended results in Table 10, 11, 12, and 13.

J Class-Incremental Learning Results

Table 14 presents a comparison between SHIELD and the HNET baseline in terms of adversarial robustness across four datasets: Permuted MNIST, Rotated MNIST, Split CIFAR-100, and Split miniImageNet, within the Class-Incremental Learning (CIL) setting. The results include AA under three adversarial attacks (AutoAttack, PGD, FGSM) as well as accuracy on original test samples, all reported after learning the full task sequence.

The results indicate that SHIELD consistently achieves higher adversarial robustness than HNET under AutoAttack across all datasets. On Permuted MNIST and Rotated MNIST, SHIELD shows large

Table 10: Comparisons of AA and BWT (only for original samples) after learning all the tasks on Permuted MNIST dataset. The results for baselines were extracted from Table 1 in (Ru et al. 2024).

Method	Permuted MNIST				
	AutoAttack	PGD	FGSM	Original samples	
	AA(%)	AA(%)	AA(%)	AA(%)	BWT
SGD	14.1	15.4	21.8	36.8	-0.66
SI	14.3	16.5	22.3	36.9	-0.67
A-GEM	14.1	19.7	22.9	48.4	-0.54
EWC	39.4	43.1	50.0	84.9	-0.12
GEM	12.1	75.5	72.8	96.4	-0.01
OGD	19.7	24.1	26.0	46.8	-0.57
GPM	70.4	72.9	65.7	97.2	-0.01
DGP	81.6	81.2	75.8	97.6	-0.01
SHIELD	80.91 \pm 1.18	90.11 \pm 0.8	78.87 \pm 2.06	93.58 \pm 0.52	0.02 \pm 0.01
SHIELD _{IM}	80.08 \pm 0.01	97.44 \pm 0.05	79.09 \pm 0.87	97.96 \pm 0.04	-0.05 \pm 0.03

Table 11: Comparisons of AA and BWT (only for original samples) after learning all the tasks on Rotated MNIST dataset. The results for baselines were extracted from Table 2 in (Ru et al. 2024).

Method	Rotated MNIST				
	AutoAttack	PGD	FGSM	Original samples	
	AA(%)	AA(%)	AA(%)	AA(%)	BWT
SGD	14.1	9.9	20.4	32.3	-0.71
SI	13.9	15.3	20.1	33.0	-0.72
A-GEM	14.1	21.6	24.8	45.4	-0.57
EWC	45.1	49.5	46.5	80.7	-0.18
GEM	11.9	76.5	74.4	96.7	-0.01
OGD	19.7	23.8	23.8	48.0	-0.55
GPM	68.8	71.5	65.9	97.1	-0.01
DGP	81.6	82.6	78.6	98.1	-0.00
SHIELD	85.64 \pm 0.03	92.94 \pm 0.16	83.82 \pm 0.2	95.62 \pm 0.06	-0.03 \pm 0.05
SHIELD _{IM}	82.91 \pm 0.37	97.88 \pm 0.08	83.03 \pm 0.45	98.32 \pm 0.06	-0.08 \pm 0.04

margins of improvement across all attack types, with particularly high AA under PGD on Permuted MNIST (97.21%) and AutoAttack (36.9%) on Rotated MNIST. For Split CIFAR-100, both methods perform similarly. On the more challenging Split miniImageNet benchmark, SHIELD again significantly outperforms HNET in all scenarios, achieving over 12% of AA under AutoAttack compared to just 2% for the baseline.

These findings confirm that SHIELD offers a substantial improvement in adversarial robustness in continual learning, even under challenging conditions. Notably, this is the first method, to our knowledge, that demonstrates strong robustness against adversarial attacks in the CIL setting, highlighting the practical effectiveness and novelty of the proposed framework.

The results reported in Table 14 were averaged over multiple random seeds to ensure statistical reliability. Specifically, results for Permuted MNIST, Rotated MNIST, and Split CIFAR-100 were averaged over 5 seeds, while Split miniImageNet results were averaged over 3 seeds. Due to the computational cost of AutoAttack, its results were averaged over 2 seeds for all datasets.

We present the pseudocode for SHIELD in the CIL

setting in Algorithm 1. During inference, since task identity is unknown, the hypernetwork generates task-specific models for all tasks, and each is evaluated on the given input. The task is inferred by selecting the model with the lowest predictive entropy, assuming that the correct task model yields the most confident prediction. When adversarial attacks are considered, task inference is always performed on perturbed inputs to simulate realistic evaluation conditions. A prediction is counted as correct only if both the task is correctly inferred and the predicted class matches the true label; otherwise, it is treated as misclassified.

K Training Algorithm

The training procedure of SHIELD is detailed in Algorithm 2. Note that subtracting a scalar from a tensor denotes a broadcasted operation, where the scalar is automatically expanded to match the shape of the tensor. This broadcasting allows element-wise arithmetic without the need for explicit reshaping. In particular, such operations occur during the construction of perturbed inputs (e.g., interval bounds), enabling efficient implementation.

Table 12: Comparisons of AA and BWT (only for original samples) after learning all the tasks on Split CIFAR-100 dataset. The results for baselines were extracted from Table 3 in (Ru et al. 2024).

Method	Split CIFAR-100				
	AutoAttack	PGD	FGSM	Original samples	
	AA(%)	AA(%)	AA(%)	AA(%)	BWT
SGD	10.3	12.8	19.4	46.5	-0.49
SI	13.0	15.2	19.8	45.4	-0.48
A-GEM	12.6	12.9	20.7	40.6	-0.48
EWC	12.6	23.2	30.5	56.8	-0.35
GEM	21.2	19.4	47.7	60.6	-0.13
OGD	11.8	14.1	18.9	44.2	-0.50
GPM	34.4	36.6	53.7	58.2	-0.10
DGP	36.6	39.2	48.0	67.2	-0.13
SHIELD	60.91	59.77	45.37	64.24	-0.34
SHIELD _{IM}	63.08 ± 0.64	62.39 ± 0.38	46.48 ± 0.33	67.45 ± 0.28	-0.41 ± 0.19

Note: In the original Table 3 from (Ru et al. 2024), the reported accuracy for FGSM was higher than for original samples, which is inconsistent with expected adversarial behavior. We assume this was a mistake and have swapped the columns accordingly for a fair comparison.

Table 13: Comparisons of AA and BWT (only for original samples) after learning all the tasks on Split miniImageNet dataset. The results for baselines were extracted from Figure 3 in (Ru et al. 2024).

Method	Split miniImageNet				
	AutoAttack	PGD	FGSM	Original samples	
	AA(%)	AA(%)	AA(%)	AA(%)	BWT
SGD	20.5	22.0	23.5	30.8	-0.24
A-GEM	19.0	19.8	21.2	29.2	-0.28
EWC	21.3	22.7	24.3	29.9	-0.25
SI	20.4	21.3	22.7	28.1	-0.27
GEM	22.3	23.8	25.4	31.8	-0.20
OGD	17.9	18.8	20.7	29.6	-0.29
GPM	26.3	27.1	28.8	36.8	-0.12
DGP	32.1	33.8	35.5	44.8	-0.05
SHIELD	56.22 ± 0.37	56.8 ± 0.95	53.08 ± 0.63	59.52 ± 0.67	-0.16 ± 0.3
SHIELD _{IM}	57.9 ± 3.08	58.47 ± 1.9	54.1 ± 2.42	62.67 ± 1.9	-0.18 ± 0.43

L Training Time of SHIELD

Table 15 reports the training time of SHIELD model across different datasets. The durations are shown in the HH:MM:SS format and include standard deviations where available. For Permuted MNIST, Rotated MNIST, Split CIFAR-100, and Split miniImageNet, results are averaged over 5 training runs using the best-performing hyperparameters. For TinyImageNet, the time is reported from a single run with no standard deviation.

M Interval MixUp Samples

Figure 9 presents representative examples of samples generated using Interval MixUp. Each row corresponds to a single mixed input (the center of a hypercube), and each column shows perturbations with increasing noise magnitude. The samples were randomly selected from the Split miniImageNet dataset. This visualization highlights how the neighborhood around each mixed

point is explored, showing that small perturbations preserve the semantic content of the image, while larger ones introduce gradual variations.

Table 14: Adversarial robustness of SHIELD across multiple datasets in the CIL scenario. We report AA under AutoAttack, PGD, and FGSM attacks, as well as on original samples after learning all tasks.

Dataset	Method	AutoAttack	PGD	FGSM	Original samples
Permuted MNIST	SHIELD	79.76 ± 0.18	97.21 ± 0.32	77.76 ± 1.5	97.46 ± 0.27
	HNET	3.96 ± 2.45	89.16 ± 0.92	12.02 ± 0.26	93.97 ± 0.49
Rotated MNIST	SHIELD	36.9 ± 0.21	39.12 ± 0.47	12.01 ± 0.28	42.32 ± 0.56
	HNET	7.77 ± 0.07	31.86 ± 0.75	3 ± 0.36	38.64 ± 0.8
Split CIFAR-100	SHIELD	15.17 ± 0.23	13.08 ± 0.43	9.8 ± 0.47	23.11 ± 0.44
	HNET	10.57 ± 0.21	13.47 ± 0.5	11.91 ± 0.45	21.15 ± 0.69
Split miniImageNet	SHIELD	12.66 ± 0.88	9.65 ± 1.79	9.53 ± 1.76	19.16 ± 1.25
	HNET	2.06 ± 0.42	4.33 ± 0.76	6.19 ± 0.92	12.84 ± 2.53

Algorithm 1: The pseudocode of SHIELD in CIL setting

Require: Trained task embeddings $\{e_t\}_{t=1}^T$, number of tasks T , trained hypernetwork $\mathcal{H}(\cdot; \Phi)$ with weights Φ , test sample x , number of classes C_t per task

Ensure: Predicted label \hat{y} and inferred task ID \hat{t}

- 1: **for** $t = 1$ to T **do**
- 2: $\theta_t \leftarrow \mathcal{H}(e_t; \Phi)$
- 3: $\hat{y}^{(t)} \leftarrow \text{Softmax}(f(x; \theta_t))$
- 4: Compute entropy: $\psi_t \leftarrow -\sum_{j=1}^{C_t} \hat{y}_j^{(t)} \cdot \log(\hat{y}_j^{(t)})$
- 5: **end for**
- 6: $\hat{t} \leftarrow \arg \min_t \psi_t$
- 7: $\hat{y} \leftarrow \arg \max_j \hat{y}_j^{(\hat{t})}$

Table 15: Comparison of training time of the SHIELD model on considered datasets.

Dataset	SHIELD
Permuted MNIST	00 : 37 : 59 ± 00 : 00 : 02
Rotated MNIST	00 : 36 : 18 ± 00 : 00 : 19
Split CIFAR-100	02 : 10 : 23 ± 00 : 02 : 00
Split miniImageNet	09 : 21 : 05 ± 00 : 12 : 11
TinyImageNet	05 : 16 : 04

Algorithm 2: The pseudocode for SHIELD training

Require: Task embeddings $\{\mathbf{e}_t\}_{t=1}^T$, hypernetwork $\mathcal{H}(\mathbf{e}_t; \Phi)$, target network $f(\cdot; \mathcal{H}(\mathbf{e}_t; \Phi))$, number of tasks T , training data $D_t = \{(x_i, y_i)\}_{i=1}^{N_t}$, regularization weight $\beta > 0$, perturbation value ε , cross-entropy weight $\kappa \in (0, 1)$, number of training steps n , Beta distribution parameter $\alpha \geq 0$

Ensure: Trained parameters Φ and $\{\mathbf{e}_t\}_{t=1}^T$

```
1: Randomly initialize  $\Phi$  and  $\{\mathbf{e}_t\}_{t=1}^T$ 
2: for  $t = 1$  to  $T$  do
3:   if  $t > 1$  then
4:     Freeze  $\mathbf{e}_{t-1}$ 
5:     for  $j = 1$  to  $t - 1$  do
6:        $\theta_j \leftarrow \mathcal{H}(\mathbf{e}_j; \Phi)$ 
7:     end for
8:   end if
9:    $\varepsilon' \leftarrow 0$ 
10:   $\kappa' \leftarrow 1$ 
11:  for step = 1 to  $n$  do
12:     $\theta_t \leftarrow \mathcal{H}(\mathbf{e}_t; \Phi)$ 
13:    Sample minibatch  $\{(x_i, y_i)\}_{i=1}^B$  from  $D_t$ 
14:    Sample  $\lambda \sim \text{Beta}(\alpha, \alpha)$ 
15:     $\varepsilon_{\text{IM}} \leftarrow |2\lambda - 1| \cdot \varepsilon'$ 
16:    Sample  $x_i \neq x_j$  from minibatch
17:     $\tilde{x} \leftarrow \lambda \cdot x_i + (1 - \lambda) \cdot x_j$ 
18:     $[\hat{y}, \bar{y}] \leftarrow f([\tilde{x} - \varepsilon_{\text{IM}}, \tilde{x} + \varepsilon_{\text{IM}}]; \theta_t)$ 
19:     $\hat{y} \leftarrow f(\tilde{x}; \theta_t)$ 
20:    if  $t = 1$  then
21:       $\mathcal{L}_{\text{total}} \leftarrow \mathcal{L}_{\text{MixUp}}$  {From Eq. (16), using  $\varepsilon'$ 
        and  $\kappa'$ }
22:    else
23:       $\mathcal{L}_{\text{total}} \leftarrow \mathcal{L}_{\text{MixUp}} + \beta \cdot \mathcal{L}_{\text{out}}$  {From Eq. (11),
        using  $\varepsilon'$  and  $\kappa'$ }
24:    end if
25:    Update  $\Phi$  and  $\mathbf{e}_t$  using gradient descent
26:    if step  $\leq \lfloor \frac{n}{2} \rfloor$  then
27:       $\varepsilon' \leftarrow \varepsilon \cdot \frac{2 \cdot \text{step}}{n}$ 
28:       $\kappa' \leftarrow \max\{\frac{1}{2}, 1 - \frac{\text{step}}{2n}\}$ 
29:    end if
30:  end for
31:  Store  $\mathbf{e}_t$ 
32: end for
```



Figure 9: Each row corresponds to a single Interval MixUp-generated sample (hypercube center), and each column shows perturbations with increasing noise magnitude. This visualization demonstrates how added noise affects interpolated inputs, preserving semantic structure under small perturbations and gradually introducing variability.